May 2016

Synthesis of LiFePO4/C Cathode Nanomaterials for Lithium-Ion Batteries

Chao Cheng
University of Wisconsin-Milwaukee

SYNTHESIS OF $LiFePO_4$/C CATHODE NANOMATERIALS FOR LITHIUM-ION BATTERIES

by

Chao Cheng

A Thesis Submitted in
Partial Fulfillment of the
Requirements for the Degree of

Master of Science
in Engineering

at

The University of Wisconsin-Milwaukee
May 2016

ABSTRACT

SYNTHESIS OF $LiFePO_4$/C CATHODE NANOMATERIALS FOR LITHIUM-ION BATTERIES

by

Chao Cheng

The University Of Wisconsin-Milwaukee, 2016
Under the Supervision of Dr. Junjie Niu

Lithium-ion batteries have been widely used for many years. The wide application covers such as smart phones, laptops, digital cameras, MP3 players, and electric vehicles. Lithium-ion batteries have become the most important energy storage device in the future. For lithium-ion batteries, the performance of the cathode materials is one of the most important factors. In recent years, the cathode materials have been widely studied including $LiCoO_2$, $LiNiO_2$, $LiMnO_2$, $LiMn_2O_4$ and phosphate etc. Among the olivine structure cathode materials, the $LiFePO_4$ (LFP) displays an excellent electrochemical activity and a chemical stability which ensure a high safety. In order to better improve the battery performance, a thorough understanding of phase transformation during the charge/discharge in real time poses a critical issue on this promising battery. Here we applied a template-assisted CVD method to synthesize LFP nanomaterials. In this experiment, we aim to synthesize nano-sized hollow sphere LFP/C structure. $LiC_2H_3O_2{\cdot}2H_2O$ (Sigma-Aldrich), $Fe(NO_3)_3{\cdot}9H_2O$ (Sigma-Aldrich), H_3PO_4 (Sigma-Aldrich) are used as the reactants. Colloidal silica (Nissan Chemical) is used as the nano-sized sphere template. The sucrose (Sigma-

Aldrich) is used as the source of the carbon. The collison nebulizer (BGI) is used to spray the aqueous solution as liquid drop state into the tube furnace. Under the argon flow, black powders are collected using the filter holder (VWR). After annealing, LFP is collected. Then removing the SiO_2 template is an important step. A variety of characterizations (XRD, SEM, TEM), electrochemical measurements and transmission X-ray microscopy (TXM) have been used to test the cathode materials.

TABLE OF CONTENTS

LIST OF FIGURES

LIST OF TABLES

LIST OF ABBREVIATIONS

$LiFePO_4$ ---------- LFP

deionized water ---------- DI water

X-ray diffraction ---------- XRD

Scanning electron microscope ---------- SEM

Transmission electron microscopy ---------- TEM

High-resolution transmission electron microscopy ---------- HRTEM

Transmission X-ray microscopy ---------- TXM

Cyclic voltammetry ---------- CV

Polyvinylidene fluoride ---------- PVDF

N-methyl-2-pyrrolidone ---------- NMP

X-ray absorption near edge structure ---------- XANES

ACKNOWLEDGMENTS

I would like to thank my advisor, Dr. Junjie Niu. He supports me to finish my thesis project. His encouragement and new ideas help me overcome many difficulties. His rigorous academic attitude educates me what is a researcher should do.

I also want to thank the members in Dr. Niu's group. Special thanks to Yan Zhang and Shuai Kang. They help me a lot and give me many advices.

I also thank Dr. Yin Wang and Dr. Benjamin Church.

Finally, I want to appreciate my parents. They understand me and support me to finish my graduate studies.

Chapter 1 – Introduction

1.1 Lithium-ion battery

Lithium-ion batteries (LIB) have long been studied and developed as power source for portable devices[1]. As a member of rechargeable batteries, lithium-ion batteries are widely used. The wide application covers such as smart phones, laptops, digital cameras, MP3 players, and electric vehicles. Lithium-ion batteries have become the most important energy storage device of the future[2]. Batteries consist of three parts. They are positive electrode (anode or + terminal), negative electrode (cathode or - terminal), and electrolyte. Lithium-ion batteries working principle is because of the different concentration of lithium content between the anode and cathode of the battery. When charging the battery, Li^+ moves from the cathode to anode. Discharging will cause the inverse movement of Li^+. In the discharge process, the anode materials have electrochemical oxidation reaction. In the electrochemical oxidation reaction process, Li ions are released into the electrolyte. Li ions can travel across the electrolyte and be absorbed by the cathode. At the same time, electrons move through the external circuit then travel towards the cathode. When we charge the battery this process is reversed.

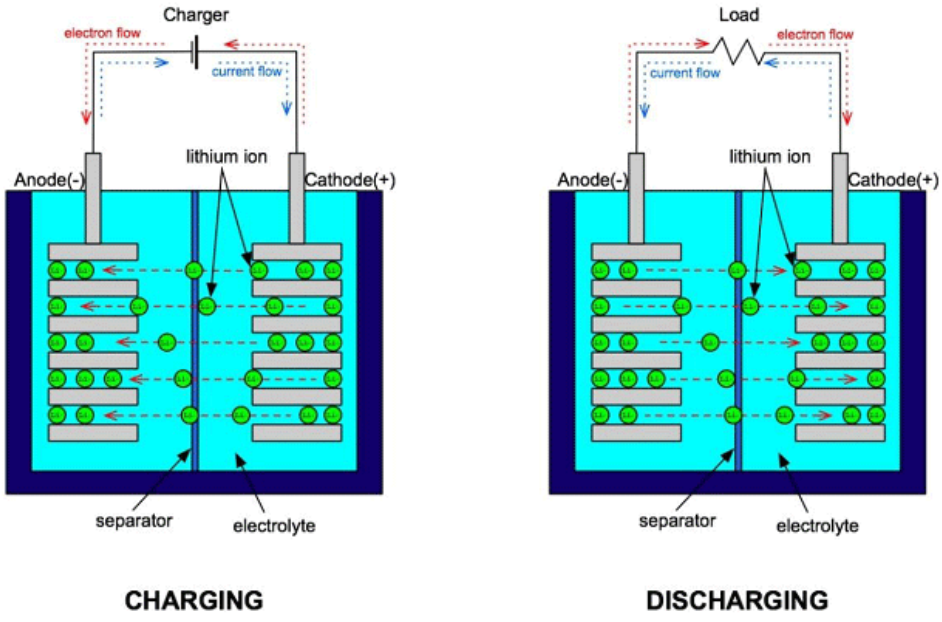

Figure 1. How lithium-ion battery produces electricity.

So use LFP as an example to show the charging and discharging equation of LIB is[3]:

Charge: $LiFePO_4 - x\ Li^+ - x\ e^- \rightarrow x\ FePO_4 + (1-x)\ LiFePO_4$

Discharge: $FePO_4 + x\ Li^+ + x\ e^- \rightarrow x\ LiFePO_4 + (1-x)\ FePO_4$

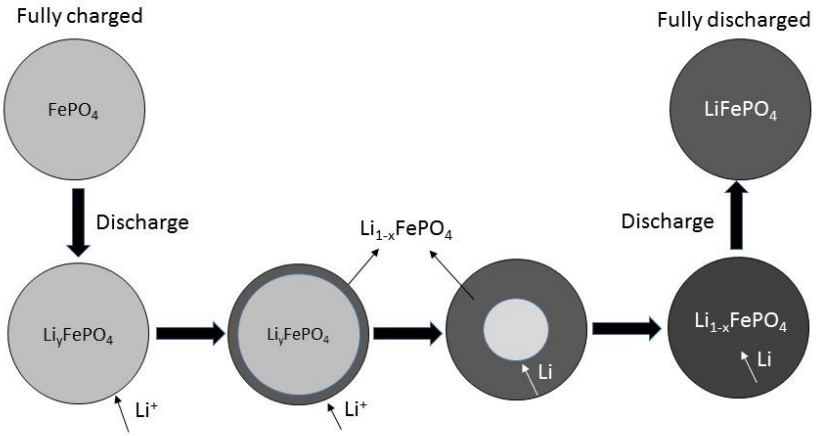

Figure 2. Li^+ insertion process (discharge process).

In order to understand the electrode materials for lithium ion batteries, some key parameters should be introduced. Such as capacity denotes charge per mass ($mAhg^{-1}$). This value can be calculated and it is an important parameter for the weight sensitive application[4]. For electrode materials, good performance means a high mass loading, high capacity loading and electrode capacity per unit area ($mAhcm^{-2}$). And for the majority of applications, the volumetric capacity ($mAhcm^{-3}$) is also an important parameter. The charge/discharge rate of the electrode is more important for commercial viability. This parameter is reported as c-rate. Cycle life and electrode potential are other parameters for the electrode performance. Cycle life measure a battery's life. It means how many charge/discharge cycles a battery could have. For electrode's potential, measured in half-cell with Li foil counter electrode during electrochemical testing, determines both safety and energy density characteristics[5].

1.2 Cathode and anode electrodes

1.2.1 Anode materials

Lithium-ion batteries have already become the best choice for the portable electronics. But there are still some limits such as available energy. An increase in battery energy density, particularly volumetric energy density, can greatly improve and expand the possibilities of portable electronics[4]. Anode and cathode materials are both important for the batteries. So much research has been done in order to improve the properties of anode and cathode. The performance of the anode materials includes energy density, power density, and cycle life. As anode materials, the lower potential it presents, the higher energy density it will have. Figure 3[5]

shows the elements which have been used for the lithium-ion batteries. The anode materials include silicon (Si), silicon dioxide (SiO_x), tin (Sn), and tin oxide (SnO_x) which have received a lot of attention from researchers. Among these anode materials, Si anodes have shown favorable properties.

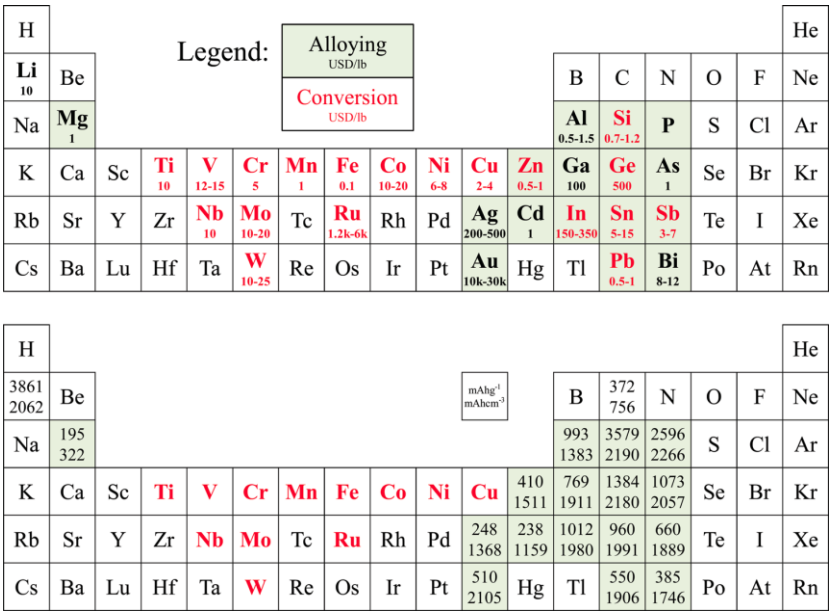

Figure 3. Elements investigated for high-capacity Li-ion battery anode materials.

1.2.2 Cathode materials

For the lithium-ion batteries, cathode materials have attracted much attention because it has an important effect on batteries. The cycle life, capacity, voltage, and safety will influence the cathode material. The structure of cathode materials is a kind of solid host framework[6]. The ions can be inserted into the framework structure and also can be removed from it. In this process, ions can be stored in the cathode materials. For lithium-ion batteries, Li^+ acts as this exotic ions.

From the previous work, the cathode materials which people have found are $LiCoO_2$, $LiMn_2O_4$, and $LiFePO_4$ etc. They mainly belong to three network structures which are layered, spinel, and olivine.

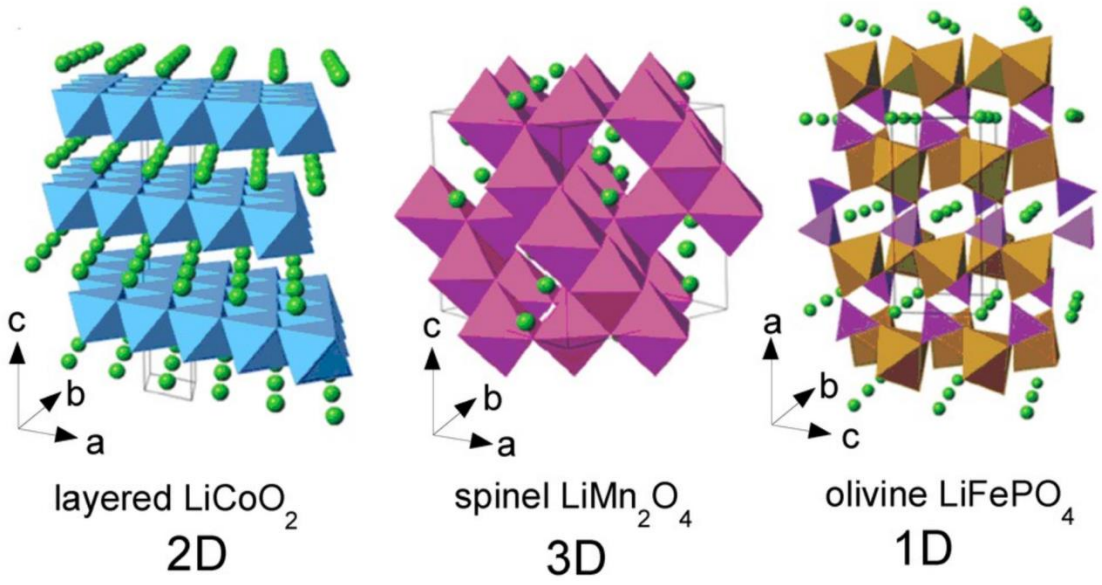

Figure 4. Li^+ transport models for layered, spinel, and olivine structures[7].

Table 1 lists the cathode materials which belong to the three frameworks. Nowadays, most researches about the cathode materials are focused on the transition metal oxide. The first transition metal oxide material is $LiCoO_2$ from 1990 when the lithium-ion batteries were invented. Its framework is layered. $LiCoO_2$ has a high theoretical specific capacity of 274 $mAhg^{-1}$, high theoretical volumetric capacity of 1363 $mAhg^{-1}$, low self-discharge, high discharge voltage, and good cycling performance[8].

Framework	Compound
Layered	$LiCoO_2$
	$LiNi_{1/3}Mn_{1/3}Co_{1/3}O_2$
Spinel	$LiMnO_4$
	$LiMn_{3/2}Ni_{1/2}O_4$
Olivine	$LiFePO_4$
	$LiFe_{1/2}Mn_{1/2}PO_4$

Table 1. Cathode materials classified by different framework[7].

Cathode	$LiCoO_2$	$LiMn_2O_4$	$LiNiO_2$	$LiFePO_4$
Capacity/$mAhg^{-1}$	274	148	274	169
Potential/V	3.90	4.05	3.6	3.40
Density/g cm^{-3}	5.10	4.31	4.85	3.60

Table 2. The comparison between different cathode materials.

But the limits of these cathode materials are high cost, low thermal stability and fast capacity fade at high current rate[6]. The spinel $LiMnO_4$'s advantage is low cost and environmental friendliness because of Mn. But the capacity and other performances are not much better than $LiCoO_2$. With the new research about the cathode materials, polyanions are developed. The

polyanions which include SO_4, PO_4, and SiO_4. They occupy the lattice positions and increase cathode redox potential[9]. The olivine structure $LiFePO_4$ is belong to the polyanions.

1.3 $LiFePO_4$ cathode materials

1.3.1 $LiFePO_4$

$LiFePO_4$ was first reported by Goodenough *et al* in 1997[10]. From the previous work, iron-based materials are much more attractive than others because Fe is cheap, abundant and less toxic. And it also has the advantage of thermal stability, very flat potentials (3.4 V) during charge and discharge processes, high theoretical capacity (170 $mAhg^{-1}$ or 610 C/g) and long cycle life[11]. After modifications such as aliovalent doping[12], size reduction[13], and carbon coating[14], LFP electrode display high rate and cycling capabilities[15]. LFP has the olivine-structure.[16] Its framework consists of FeO_6-octahedra and PO_4-octahedra. The lithium atoms occupy the interstitial voids of the framework and Li^+ and Fe^{2+} occupy octahedral sites[6].

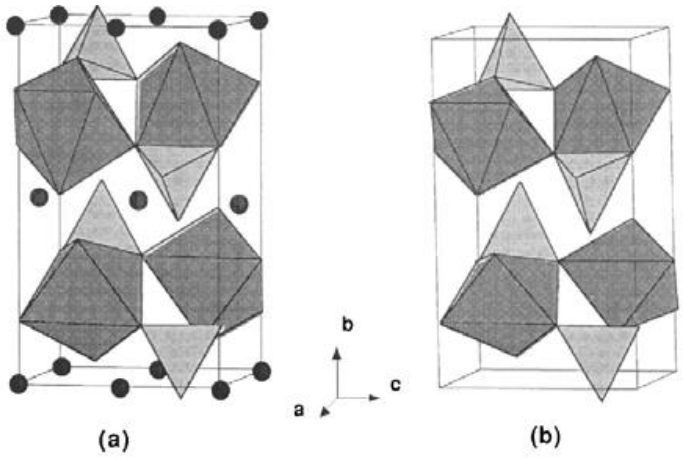

Figure 5. Crystal structure of (a) $LiFePO_4$ and (b) $FePO_4$[3].

Figure 5 shows the structure of $LiFePO_4$ and the lithium atoms' position. The phase $FePO_4$ has almost the same structure as $LiFePO_4$. When the batteries charge/discharge, the volume of the structure doesn't change so much between the $LiFePO_4$ phase and $FePO_4$ phase. This characteristic can avoid the capacity degradation and compensate the volume changes of the carbon anode during lithiation/delithiation. That's why the $LiFePO_4$ structure system can have the truly excellent electrochemical cyclability. The strong covalent P-O bonds make the oxygen stable in LFP which means O_2 will not release at high state of charging. That also causes LFP to have a good thermodynamic and dynamic state even over 200 °C temperature. This characteristic makes LFP to become a safe, stable, and good cathode material[17]. And it also can reduce the covalent bonding to the iron ion[3]. The low cost, abundance, good thermal stability, high theoretical capacity, flat potentials and environmentally benignity are all its advantages[18]. The weakness of LFP which includes low average potential and low electrical conductivity will be introduced later.

1.3.2 Li^+ extraction and insertion mechanism of $LiFePO_4$

The LFP's working principle is mainly about the diffusion process of Li^+. This diffusion process is the lithium insertion/extraction process. It is a very important process to study about the $LiFePO_4$ cathode mechanism. When the batteries charge, the Li^+ is extracted from the $LiFePO_4$ and be inserted into the anode electrode. In this charge/discharge process, two phases can be observed. $LiFePO_4$ phase and $FePO_4$ phase can exit at the same time. Li_xFePO_4 is commonly described as this two-phase reaction[19]. Laffont's research[20] proposed a new model to explain $LiFePO_4/FePO_4$ two phase transformation process. It is similar to core-shell structure models

during the charge/discharge process. During charge process, Li^+ will be extracted from the center of the particles at first. During discharge process, the insertion of Li^+ will start from the outer layer. That shows the $LiFePO_4/FePO_4$ always keeps a core-shell structure. Recently, Delmas proposed another model to describe the transformation process which is domino-cascade[21]. According to his model, when the Li^+ insertion/extraction starts in one particle, the particle will become totally charged or discharged[20]. This is different with the core-shell model from Laffont. So in this study, observing the transformation between $LiFePO_4/FePO_4$ phases during the charge/discharge process using transmission X-ray microscopy (TXM) is a significant step. The data from TXM will be listed and be explained in the result section.

1.3.3 The challenges of $LiFePO_4$

$LiFePO_4$ acting as the cathode material still has some problems. Its tap density is low. And it also shows poor low temperature performance. The tap density is defined as the mass of particles divided by the total volume the particles occupy. The theoretical density of $LiFePO_4$ is only 3.60 gcm^{-3}. From the Table 2, its density is lower than other cathode materials. In general, most $LiFePO_4$ only has 1 to 1.4 g cm^3 density[19]. For powder materials, both theoretical density and particle morphology can decide the tap density. The particle morphology includes the particle size, particle distribution, and geometric shape. Such as the smaller particle size will decrease the density, and the more carbon content will also decrease the density[19]. For $LiFePO_4$ cathode materials, small particles size and carbon coating are both important for the rate performance.

So this becomes a contradictory problem which makes the LFP's density be low. Low tap density will cause LFP has a limited used in a hand-held device.

Another poor performance is LFP'S low-temperature performance. From the 45th battery symposium report in Japan, LFP batteries will have lower capacity with the temperature down[19]. This character makes the battery can't arrive the requirement for the electric vehicles. And the electrolyte of LFP battery has the same problem. The diffusion of Li^+ is limited between electrode and electrolyte when the temperature is low, especially below -20°C.

1.3.4 Motivation

In order to improve the performance of the LFP batteries, the particle size, morphology, and carbon layer are three points which can be improved. When the particle size decreasing, Li^+ will have the shorter diffusion lengths and larger electrolyte/electrode contact area. Compared with irregular shapes, the spherical shapes can have higher tap density. There are many vacant spaces between the irregular shapes. So control the shape as sphere is so important. Carbon coating is the most effective method to improve the electronic conductivity. Compared with other coating materials such as silver or copper, carbon is much lighter and cheaper. In this experiment, we aim to synthesize nano-sized hollow sphere LFP/C structure using an easy spray method combined with CVD system. Looking for the conditions which control the morphology and particle size and studying the mechanism of Li^+ transformation are the main objective.

1.4 Silicon dioxide (SiO_2) as template

In the experiment, silicon dioxide are used as template to control the shape of LFP. The SNOWTEX-O SiO_2 template is the product of Nissan Chemical. Figure 6 is the SNOWTEX-O SiO_2 products.

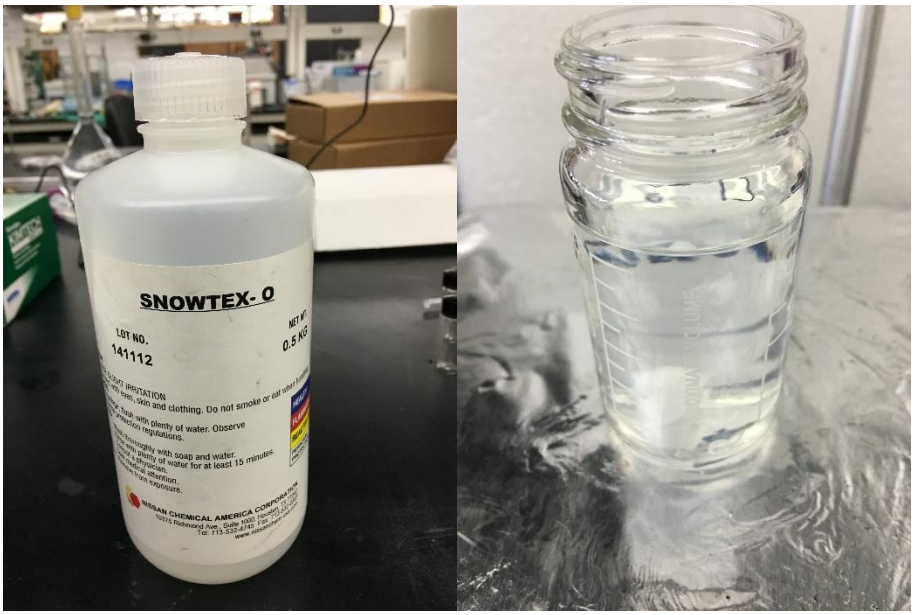

Figure 6. SNOWTEX-O colloidal silica dioxide.

The state of SiO_2 is colloidal so it can mixed with water. It is made by growing mono-dispersed, negatively charged, amorphous silica particles in water. The particle shape of SiO_2 is spherical and its particle size is 10 – 20 nm. A spherical particle can be densely packed and it is favorable for electrode processing[22]. In experiment plan, LFP will cover on the spherical SiO_2 template then carbon will be coated outside. Nano-sized particles have shorter diffusion paths for lithium ions

and electrons, which is beneficial for a fast charge/discharge capability[23]. So that's why we use such small size SiO_2 to synthesize small size LFP particles.

But there is a problem. SiO_2 has negative effect on cathode materials. Because of the SiO_2 has the electric insulation characteristic. The proportioned weight of SiO_2 is higher than LFP. That means the weight of effective cathode material is very low in one coin cell battery. The coin-cell performance will be affected and shows bad electrochemical performance. To avoid this case, remove SiO_2 will become an important step. After SiO_2 template be removed, the structure will become a hollow sphere or a porous sphere[24].

1.5 Experiment background

There are many method to synthesize LFP. Such as solid-state reaction, hydrothermal method[25], co-precipitation, emulsion-drying method, sol-gel method[26], mechanical alloying, and microwave processing[27]. In this study, an easy method to synthesize the sphere LPF/C-SiO_2 using nebulizer is adopted[28]. For the first step of the experiment, all raw materials dissolve in deionized water. The mixed chemical solution shows dark red color like Figure 7.

Figure 7. Mixed chemical solution.

In order to collect powder samples, dry and atomized the liquid chemicals is a problem which should be solved. The process of atomized can be solved by using the nebulizer equipment. Here I choose the collison nebulizer from the company BGI. Figure 8 is the sketch of the collison nebulizer. The argon gas acting as carrier can flow into the bottle from one side of the top. The design of the nebulizer can make the argon gas carrying the liquid chemicals and spraying them to become very small liquid drop. The atomized liquid will fill the whole bottle. When more vaporous is produced, it will be thrusted into the tube furnace through the outlet because of the pressure in the bottle.

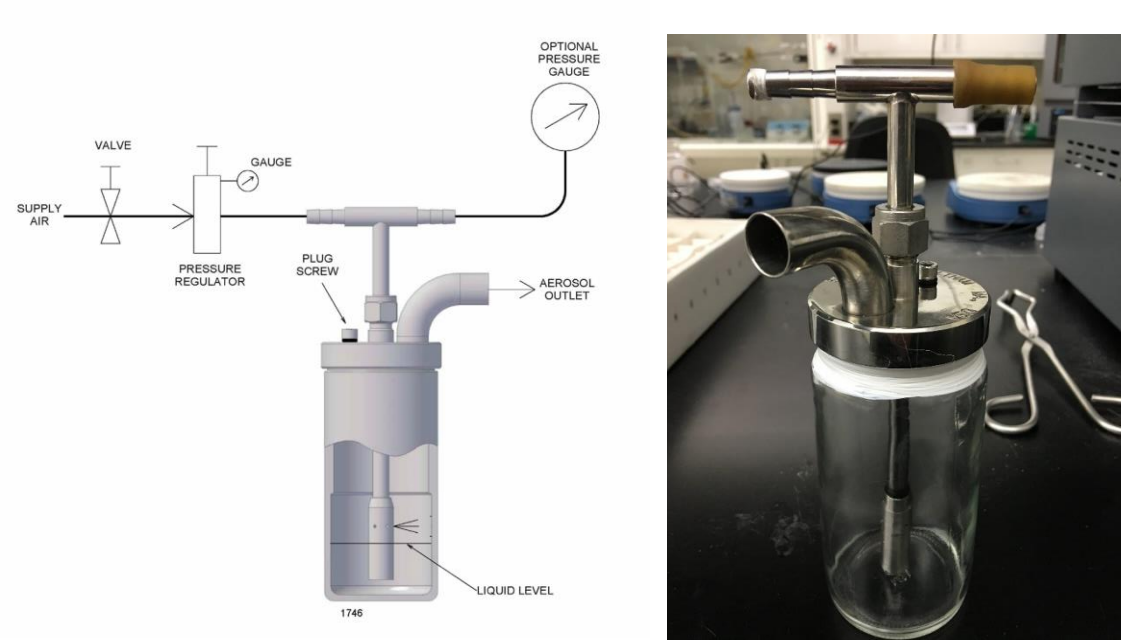

Figure 8. Sketch of the collison nebulizer.

The vacuum tube furnace is the production of MTI Corporation which is showed like figure 9. Heating the atomizing liquid drop which be sprayed from the nebulizer is the uses of tube

furnace. The temperature setting of the tube furnace should be higher than 450 °C because this temperature can dry the liquid drop chemicals and carbonize the sucrose ($C_{12}H_{22}O_{11}$)[29]. The chemical equation is listed below.

$$C_{12}H_{22}O_{11} \rightarrow 12C + 11H_2O$$

Figure 9. Tube CVD furnace.

The argon gas will bring the dried powder samples going through the quartz tube. The powder samples will be collected by the filter holders (VWR) that showed as Figure 10. The use of filter holder is mainly to contain a filter paper. The filter paper is glass microfiber filters (Whatman) which is showed as Figure 11. This kind of glass microfiber filters can collect samples under argon gas because of its good gas permeability withstand temperature over 500 °C.

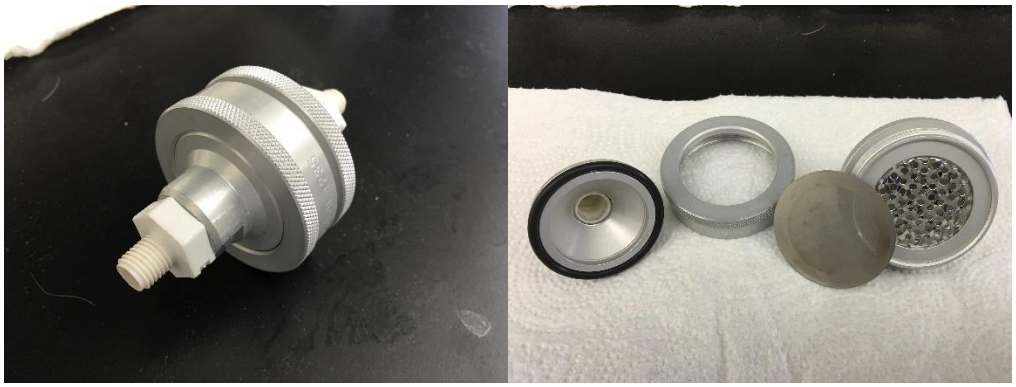

Figure 10. Filter holder for sample collection.

Figure 11. Glass microfiber filter paper (Whatman).

The argon gas carries the powder samples into one side of the filter holder. The filter paper can intercept the powder samples then the waste gas comes out from the other side of the filter holder. A tube will lead the waste gas into the fume hood. The whole experiment equipment sketch Figure 12 and real photo Figure 13 are showed below.

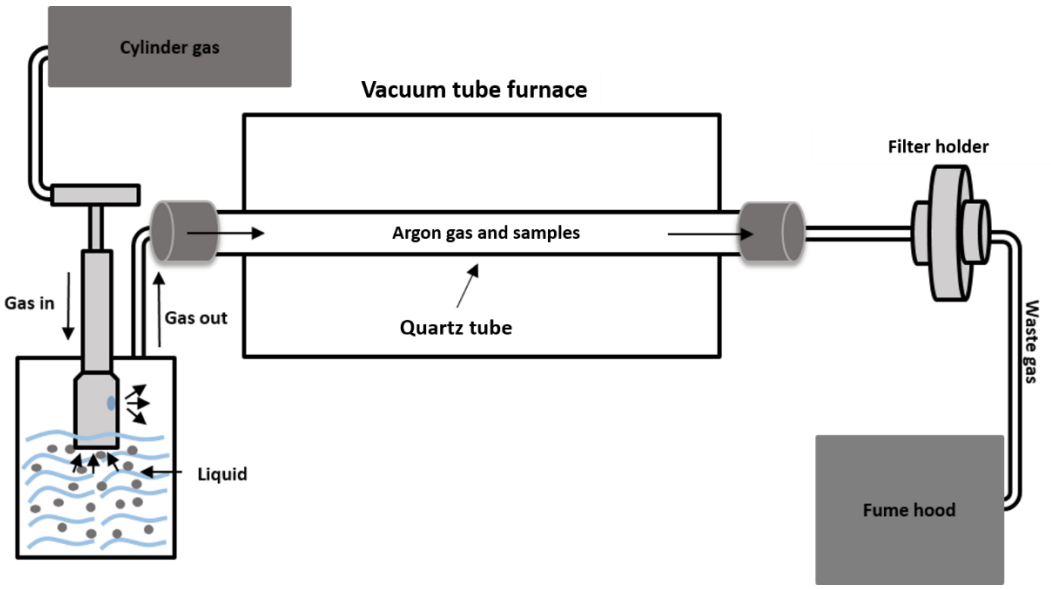

Figure 12. Process diagram of the sample synthesis.

Figure 13. Photo for the spray CVD equipment.

1.6 Background of making coin cell batteries

Coin cell battery is also called button cell or a watch battery. The size of coin cell is 5 to 25mm in dimeter and 1 to 6 mm high. Doing a coin cell battery is a common way to test the electrode materials.

Figure 14. Coin cell configurations.

Figure 14 is the configurations of the coin cell. For this experiment anode material is lithium wafer and cathode material is LFP/C-SiO_2. Doing a coin cell battery, all operations should be done in a glove box which is showed like Figure 15. Glove box is a sealed container which is allowed someone operate in it where is separate from the atmosphere.

The first step to do a coin cell battery is to prepare the LFP electrode material. Weighing the black powder samples LFP/C-SiO_2, super/P, and polyvinylidene fluoride (PVDF) as the ratio 8:1:1 on an electronic scales. LFP/C-SiO_2 samples and carbon/p are black powders. PVDF is white powder. Mix these three powders completely. Make sure there is no obvious white powders after grinding process.

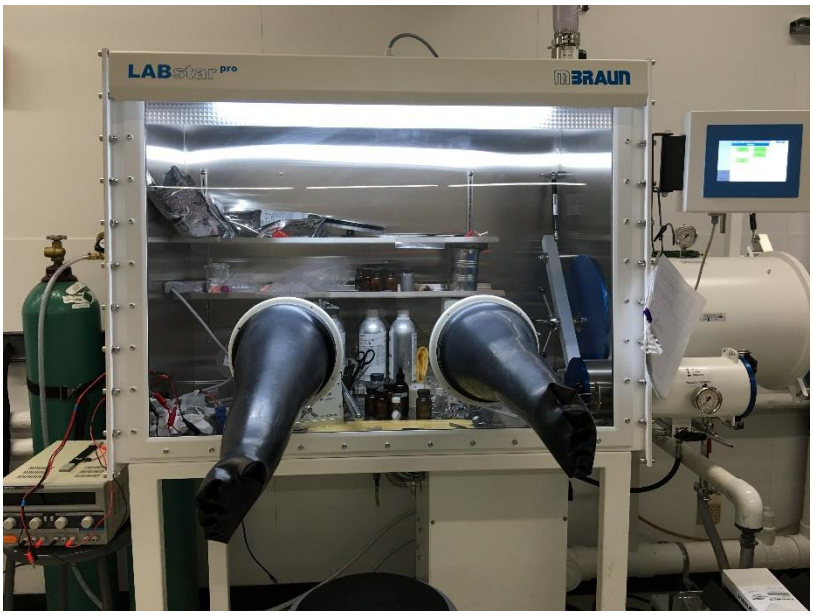

Figure 15. Glove box (Mbraun).

Then move the mixed powders into a small glass vial and add some N-methyl-2-pyrrolidone (NMP) which is binder solution. Stirring the slurry by using a magnetic stirrer for 30 minutes. After the stirring process, shake the slurry for 20 minutes in an ultrasonic machine then stir it for 2 hours again. The ultrasonic machine is showed as Figure 16. This mixing process is mainly to ensure the LFP, carbon/p, and PVDF can be mixed totally in NMP binder solution. For cathode materials, aluminum foil is selected to use as the current collector. The load weight is 10 mg/cm^2. The aluminum foil is showed as Figure 18. The loaded aluminum foil should be sent into a vacuum furnace and drying it for 12 hours. The cathode slurry and foil covered by the slurry are showed like Figure 17. The temperature of the vacuum furnace should be over 80 °C. After drying, pressing the foil by using a hydraulic press machine for 1 hour to make sure the cathode materials and aluminum foil combined strongly. Figure 19 and Figure 20 are the vacuum oven (SHELLAB) and

hydraulic press machine (STRONGWAY) photos in our laboratory. Then cut the foil to make it as cycle shape by using the ring cutter (MTI) which is like Figure 21.

Figure 16. Ultrasonic cleaner (VWR).

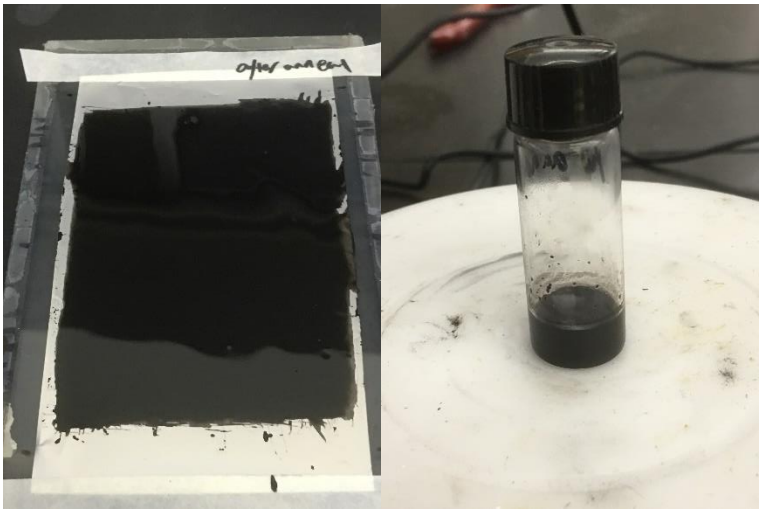

Figure 17. Images of electrode materials and slurry.

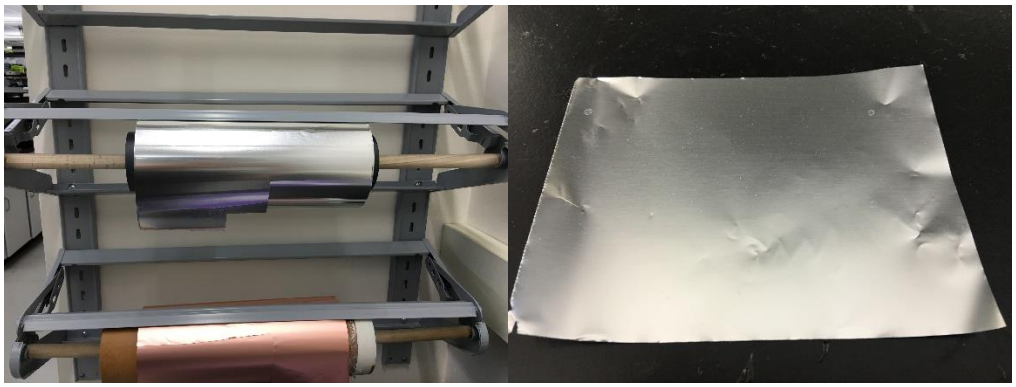

Figure 18. Aluminum foil used as the current collector.

Figure 19. Vacuum oven (SHELLAB).

Figure 20. Hydraulic press machine (STRONGWAY).

Figure 21. Ring cutter (MTI).

The size of each wafer is suitable for the coin cell battery. In order to calculate the current of each coin cell battery, the weight of each electrode material is necessary. Each wafer shape

aluminum foil after cutting is 7.7 mg. So the actual weight of electrode materials can be calculated after minus 7.7 mg.

The glove box requires vacuum pumping operation 3 times before the prepared materials need to be moved into the glove box. Assembling each coin cell battery as the Figure 14 coin cell configurations. The electrolyte is selectilyte-LP47. The electrolyte is dropped into the coin cell battery during the assembling process. Then seal the coin cell with the crimping machine which showed as Figure 22.

Figure 22. Crimping machine to seal the coin cell batteries.

The battery test system can detect coin cell batteries with different electric current. The current is a parameter which needs to be calculated according to the active mass of the cathode materials. So the weight of electrode materials which has been calculated before can be used here. The theoretical capacity of LFP is 170 mAhg^{1} with 1 C current. So for this experiment, with

the 10 mg/cm^2 loading, 0.2 C current should be 340 μA. According to the actual weight of each coin cell, work out the current for each battery and input it to the battery test equipment. The coin cell battery system is the product from the Landt Instruments vender which is showed as Figure 23.

Figure 23. Coin cell battery test system (Landt Instruments).

Chapter 2 – Experiment

2.1 Experiment chemicals

Materials	Vendor
Lithium acetate dehydrate ($LiC_2H_3O_2 \cdot 2H_2O$)	Sigma-Aldrich
Iron(III) nitrate nonahydrate ($Fe(NO_3)_3 \cdot 9H_2O$)	Sigma-Aldrich
Phosphoric acid (H_3PO_4)	Sigma-Aldrich
Sucrose ($C_{12}H_{22}O_{11}$)	Sigma-Aldrich
Collodial silicon dioxide (SiO_2)	Nissan Chemical

Table 3. The chemicals for experiments.

2.2 Experiment process

The first step of experiment is to synthesize $LiFePO_4$/C-SiO_2 samples. 12.8 g $Fe(NO_3)_3 \cdot 9H_2O$, 3.23 g $LiC_2H_3O_2 \cdot 2H_2O$, and 3.61 g H_3PO_4 are mixed in the glass beaker. The molar ratio of Li : Fe : PO_4 is 1:1:1[27]. Then add 5ml collodial SiO_2 liquid, 5 g sucrose, and 15 ml deionized water (DI-water) into the glass beaker. The colloidal SiO_2 solution should be stirred at high rotate speed for 12 hours and using ultrasound irradiation to shock it. Moving the beaker to the magnetic stirrer and stirring until all chemicals are dissolved in the DI-water. In general, the stirring progress keeps 30 minutes. The chemical solution shows dark red color. After mixing process, move the chemical

solution into the collison nebulizer equipment and assemble the main spray system equipment which include nebulizer, vacuum tube furnace, and filter holder. The temperature of the tube furnace is set at 700 °C. The collected samples are black powders. These LFP/C-SiO_2 powders have poor crystal structure because the time for the samples which stay at 700 °C temperature is too short. So the annealing process is necessary. Putting the collected samples in a quartz boat, and then do the 700 °C annealing for 6 hours in a tube furnace under the protection of argon gas. Here the collected samples is good crystal lattice LFP. Then the next step is the coin-cell battery assembling. Weigh the samples then mix with PVDF and carbon/p as the ratio 8:1:1[30]. Grinding these three powders then dissolve them in NMP solution. In order to get homogeneous slurry solution, stirring the slurry for a long time is necessary. In general, this stirring process keeps 12 hours. After stirring, the slurry is coated on the aluminum foil. The loading mass is calculated as 10 mg/cm^2. Then put the coated aluminum foil in the vacuum furnace to dry the slurry at 80 °C. After drying, pressure the foil then cut it become wafer shape by using the ring cutter. Assembling the coin-cell battery should be operated in the glove box.

Chapter 3 – Results and discussion

3.1 Effect of the temperature

In the experiment process, the first step is to synthesize good crystal structure LFP. The spraying method using nebulizer is an easy and fast way to synthesize nano-sized spherical LFP/C-SiO_2. At the initial stage of the experiment, try to find out the temperature conditions which can synthesize LFP is important. Here two different conditions were carried out. They are 450 °C and 700 °C spraying temperature.

The first condition of temperature is 450 °C. This temperature is high enough to evaporate the moisture in the sample and carbonize the sucrose. At this temperature, the collected samples are black powders. But with the XRD scanning degree from 10° to 80°, the crystal structure is really not good. The result only displays SiO_2 peak without LFP's peak. Figure 24 is the 450 °C spraying temperature XRD pattern result.

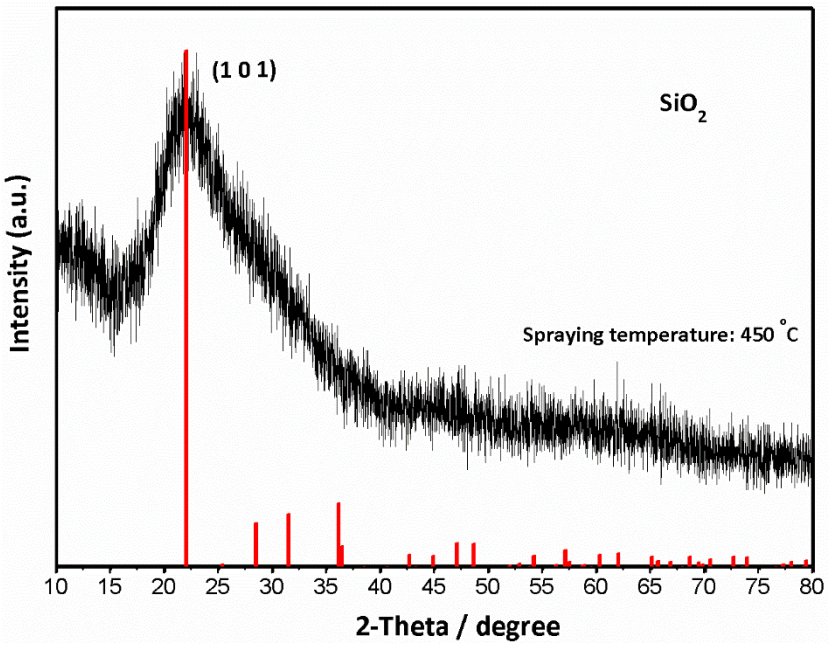

Figure 24. XRD data of the sample synthesize at 450 °C before annealing.

The most probable reason is that the residence time in the tube furnace is too short to crystallize. The control of flow rate has limit because the collison nebulizer will not work at very low flow rate. In order to improve the quality of crystal, increasing the temperature of tube furnace is an effective method. So 700 °C of the tube furnace is chosen for a contrastive experiment. Figure 25 is the XRD pattern which displays (101), (111), (211), and (311) peaks. So at the 700 °C condition, LFP has been synthesized but the sensitive of the peak is too low. That means there is LFP crystal structure in the samples, but the property is not good. From these two contrastive experiment, the conclusion is the higher spraying temperature, the better crystal structure we can get. Some other conditions will influence the crystal properties. During the spraying process, the time of the powders staying in the tube can't be controlled. So an additional step is necessary.

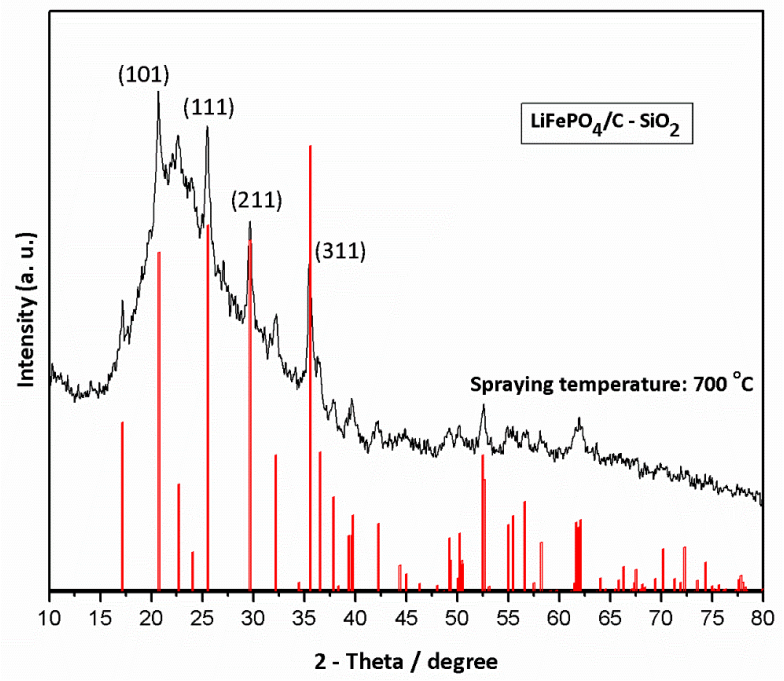

Figure 25. XRD data of the sample synthesize at 700 °C before annealing.

3.2 Effect of the annealing process

This step is the annealing process. After the spraying process, black powders are collected and do the annealing process for 6 hours at 700 °C. Figure 26 is the XRD pattern data which is after annealing process. From Figure 26, the crystal properties and the sensitive of the peak are better than before. From these three XRD patterns, the background of the patterns always has a high peak at 22.5°. Just like the pattern in Figure 24, all of the LFP's peaks are located on the SiO_2 peak.

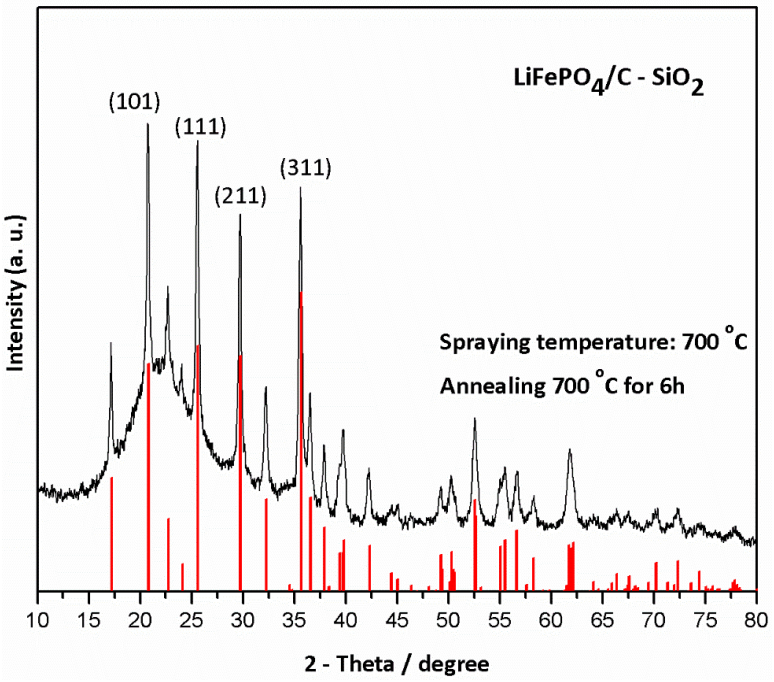

Figure 26. XRD data of the sample synthesize at 700 °C then annealed at 700 °C for 6 hours.

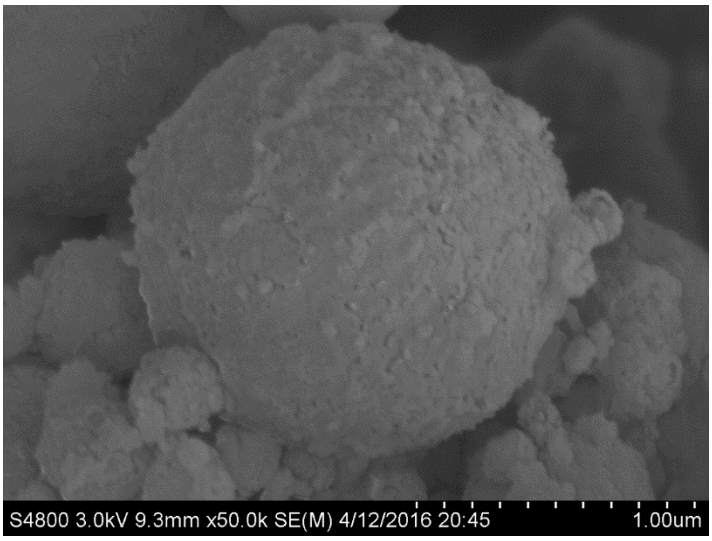

Figure 27. SEM image: $LiFePO_4$/C-SiO_2 sample before annealing process.

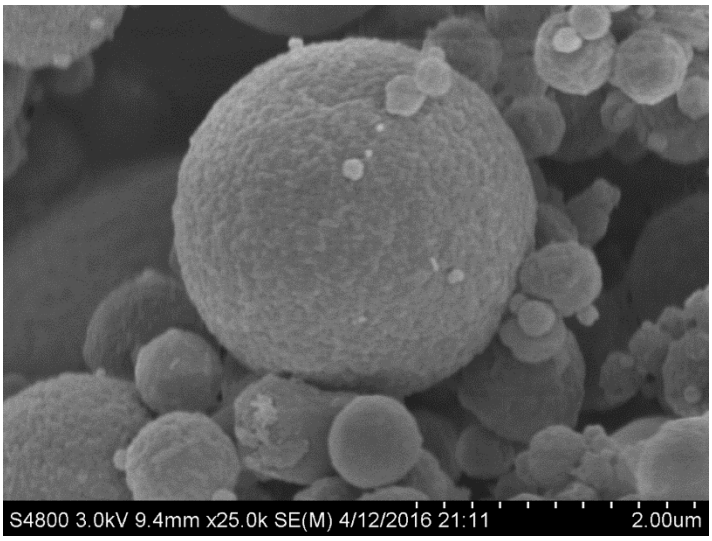

Figure 28. SEM image: $LiFePO_4$/C-SiO_2 samples after annealing process.

Figure 27 and Figure 28 are the contrastive SEM images between the annealed samples and un-annealed samples. The differences are the surface morphology and the particle size. Before annealing process, the particle size is a little bit smaller and the surface is irregular. The surface of the particles after annealing is much more regular and the particle size increases by 1-2 μm.

3.3 Effect of the SiO_2 template

In order to prove the effect of silicon dioxide in this study, I did an experiment about synthesize the LFP/C without SiO_2. Figure 29 is the LFP/C XRD pattern. Here we can see the biggest difference of the XRD patterns is the peak of SiO_2. The background of samples I did before display the peak of SiO_2. Because the SiO_2 is the template. The intensity of the peak is better than the samples which contain the SiO_2 templates. But the most difference is the shape of samples.

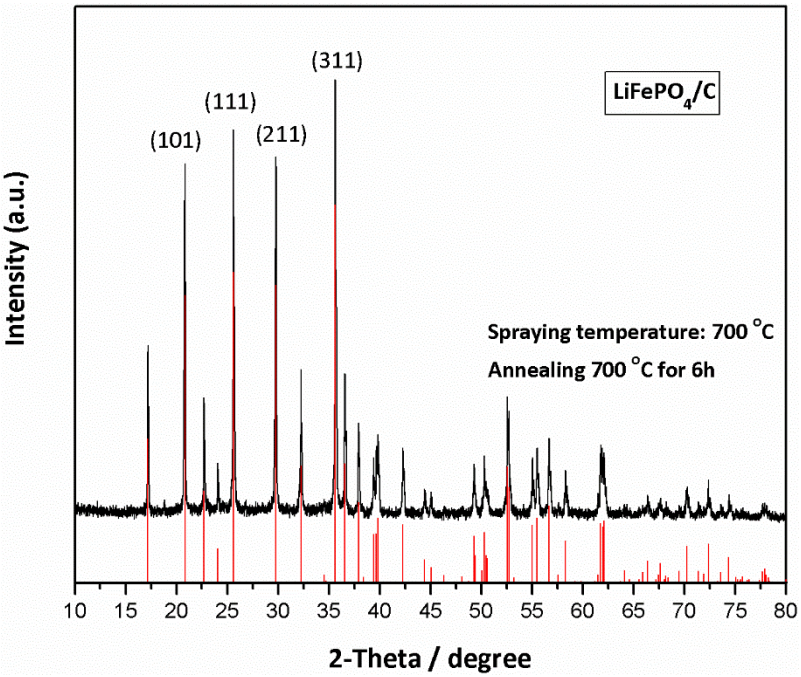

Figure 29. XRD data of the LFP/C synthesized at 700 °C then annealed at 700 °C for 6 hours.

TEM can detect very small samples at a significantly higher resolution. Nano scale particles and lattice of the particles can be observed through TEM. Figures 30-32 are the TEM images display the morphology of the particles. The exact scale can be detected by using the TEM, and

compared with different conditions. Here, the influence of the template SiO_2 will be detected in the synthesize process. Here three experiments were finished. All experiments conditions are invariable expect the amount of SiO_2. The difference among these experiments is the amount of SiO_2: 20 ml colloidal silicon dioxide, 5 ml colloidal silicon dioxide, and 0 ml colloidal silicon dioxide. 0 ml colloidal silicon dioxide is the samples without SiO_2 template. From Figure 30, the shape shows randomly. It is not sphere. Comparing with Figure 31 and Figure 32, the result is the SiO_2 templates can control the morphology as a sphere successfully.

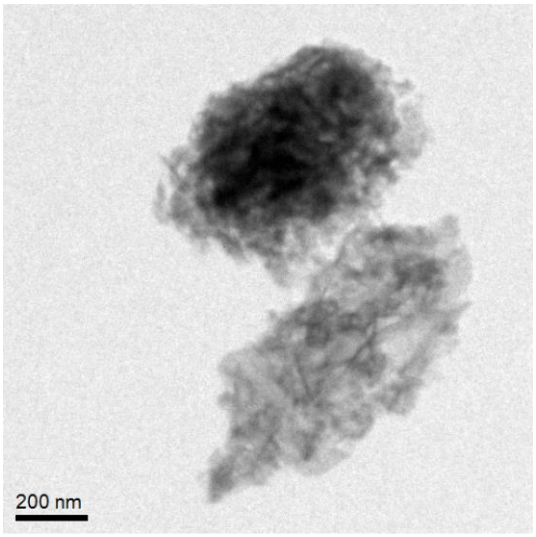

Figure 30. TEM image: Spray LFP/C without SiO_2 templates.

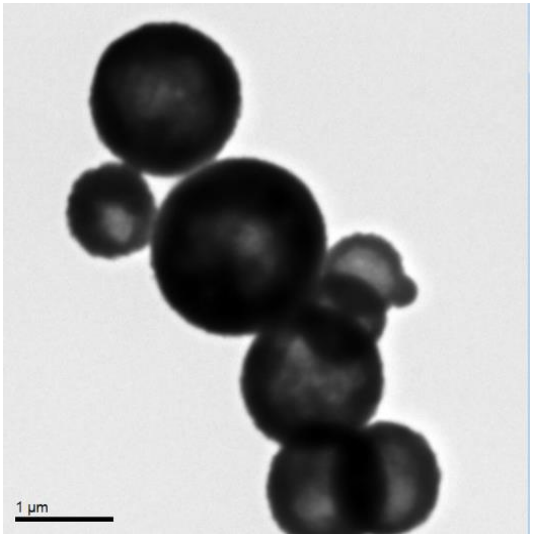

Figure 31. TEM image: Spray LFP/C with 5 ml SiO_2 as templates.

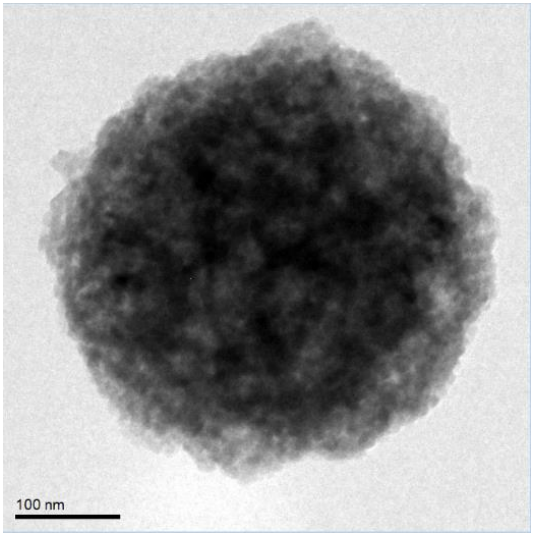

Figure 32. TEM image: Spray LFP/C with 20 ml SiO_2 as templates.

From these three experiments' results, the TEM images displays the amount of SiO_2 will have great effect on the morphology of structure and size dimension. With no SiO_2 templates, the collected samples is LPF/C but the shape is not spherical. It is irregular shape. With 5 ml SiO_2 templates, the spherical shape comes back and the average size of the particles is around 1 µm.

With 20 ml SiO_2 templates, the particle size reduce to around 300 nm. So from these three contradistinctive experiments, SiO_2 can decided the form and particle size of the LFP samples. The reason is with more amount of SiO_2, the single template SiO_2 will also increase. For one experiment, the total amount of LFP/C chemical solution is certain. With the amount of template increasing, LFP/C can has more base point to grow. That means each single SiO_2 template will get less LFP/C. So the single particle size will decrease.

The conclusion is clear. The SiO_2 templates can not only control the shape of the LFP/C, but also can control the particle size of the LFP/C.

3.4 Effect of the sucrose

Sucrose is the source of carbon. For LFP, carbon coating is the most common and effective way to increase the electronic conductivity[31, 32]. Many researches have proved this[32]. And it is necessary to synthesize LFP. The protection gas for synthesis LFP should be the mixed gas of 90% N_2 and 10% H_2[33]. But in this experiment, the protection is only Ar_2 gas. The mixed gas is mainly to prevent LFP oxidation because H_2 has reducibility. So without H_2, carbon is necessary for the LFP synthesize because carbon also has reducibility. Figure 33 is the experiment to synthesize LFP without sucrose.

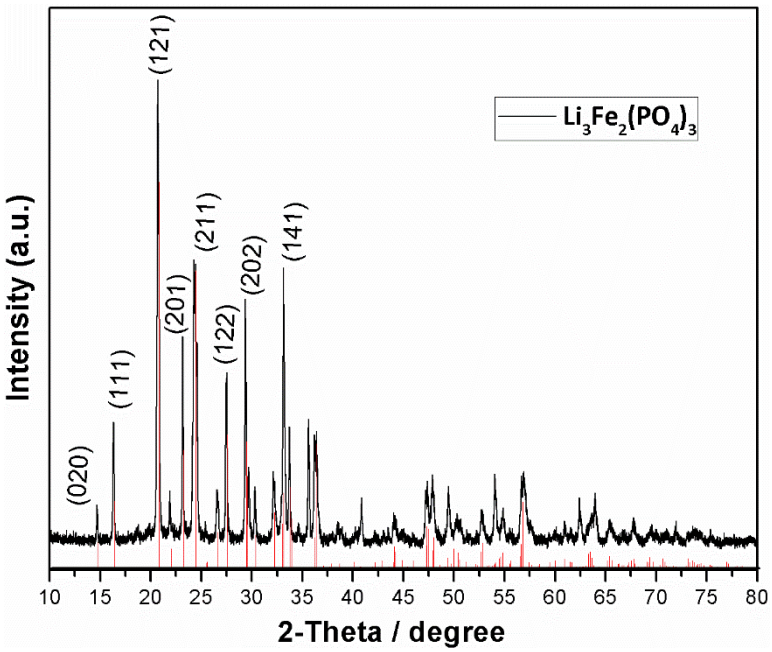

Figure 33. XRD data of the $Li_3Fe_2(PO_4)_3$ synthesized at 700 °C then annealed at 700 °C for 6 hours.

The valence of Fe is different between $Li_3Fe_2(PO_4)_3$ and $LiFePO_4$. As cathode for the batteries are also different. The theoretical specific capacity of $Li_3Fe_2(PO_4)_3$ is 128 $mAhg^{-1}$. $LiFePO_4$ has 170 $mAhg^{-1}$. So in order to get $LiFePO_4$, sucrose is necessary.

The condition of the synthesis process is confirmed. To get good crystal structure of LFP, high spraying temperature and annealing process are necessary. And carbon source is also important in the synthesis process. The SiO_2 templates can control the morphology and size of the particles.

3.5 Etching SiO_2

Now the samples are LFP/C-SiO_2. For cathode materials act as electrode, SiO_2 has negative effect for the electrochemical performance. So how to remove silicon dioxide is a big problem. As

we know, the most effective chemicals to remove silicon dioxide are sodium hydroxide (NaOH) and hydrofluoric acid (HF). Here the chemical equation can listed.

$$SiO_2 + 4HF \rightarrow SiF_4 + 2H_2O$$

$$SiO_2 + 4NaOH \rightarrow Na_4SiO_4 + 2H_2O$$

HF is strong acid and it will have reaction with LFP. The crystal lattice can be destroyed by HF. So HF solution can't be used here. Lim.[33] synthesized LFP nanowires using SiO_2 templates and he removed templates by using NaOH. So in my experiment, removing SiO_2 by using NaOH becomes an important and probable step that can be tried. The different conditions can be controlled are the etching time, the etching temperature and the NaOH concentration. The temperature for the etching is constant at 80 °C. Heating can help the reaction between SiO_2 and NaOH. Table 4 is the different etching conditions I have tried in the experiment.

Etching solution	Etching time	Etching temperature
0.5 mol/L NaOH	0.5 ~ 2 hours	80°C
1.0 mol/L NaOH	0.5 ~ 2 hours	80°C
2.0 mol/L NaOH	0.5 ~ 2 hours	80°C

Table 4. Different conditions in etching process.

In one experiment, the etching condition is 1.0 mol/L NaOH, 80 °C, and 2 hours. Here, we dissolve 20 g solid NaOH pellets in 500 ml DI-water. In this way we can get 1.0 mol/L NaOH. Figure

34(a) is the XRD pattern The $LiFePO_4/C\text{-}SiO_2$ is the samples after annealing without etching. It displays good XRD crystal lattice of LFP. Then do the etching process on this samples. The XRD pattern displays as the Figure 34 (b). The difference between these two figures is obviously. Figure 34 (b) doesn't display the characteristic of LFP. But the peak of SiO_2 is also weak. That means 1.0 mol/L NaOH solution can remove SiO_2, and it can destroy the crystal lattice structure at the same time. The TEM images can conform this result.

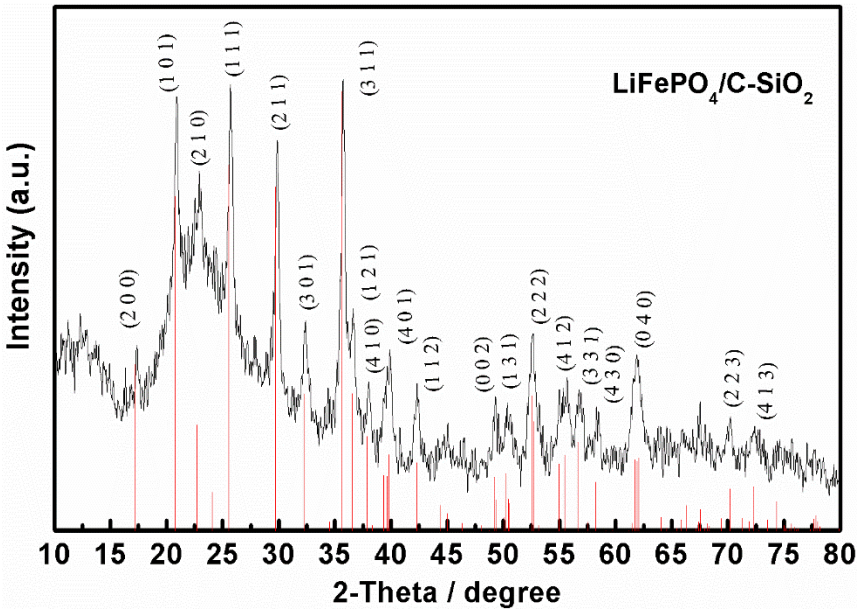

Figure 34 (a). XRD pattern: LFP/C-SiO_2 before etching.

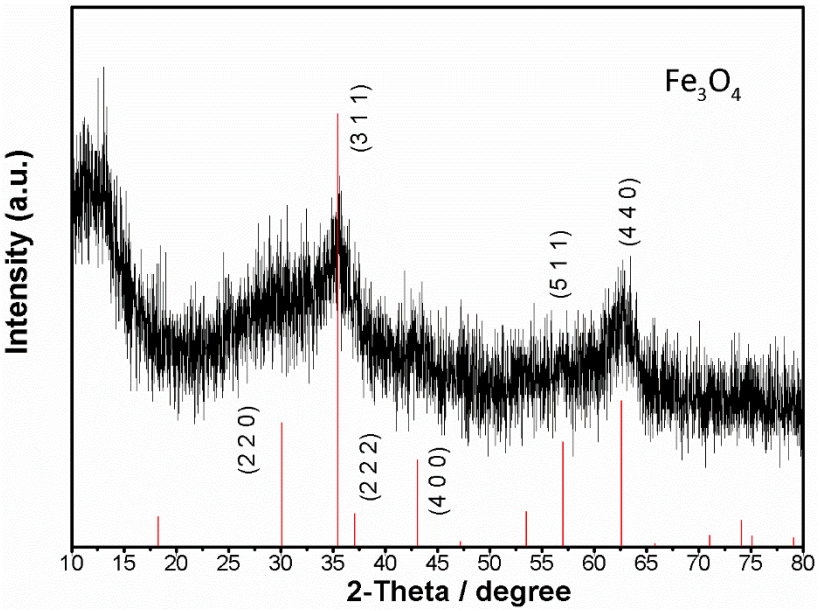

Figure 34 (b). XRD pattern: LFP/C-SiO_2 after etching using NaOH in DI-water.

Figure 35 and Figure 36 are two TEM images. Figure 35 is the LFP/C-SiO_2 without etching process. From Figure 35, the sphere particles are displayed as black solid sphere. There is no space in the center of sphere.

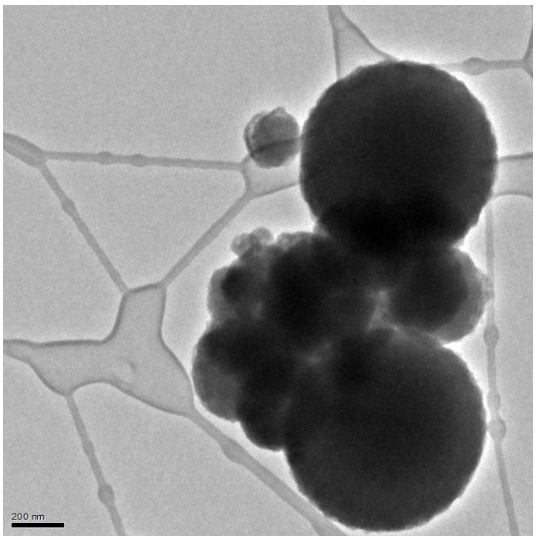

Figure 35. TEM image of LFP/C-SiO_2 before etching.

Figure 36 is the particles which are suffered etching process. The TME image displays the obvious space in the center of the sphere that just likes hollow sphere. At the same time, a lot of broken sphere can be observed. That means the etching condition is so strong. So it is necessary to change the condition of the etching experiment.

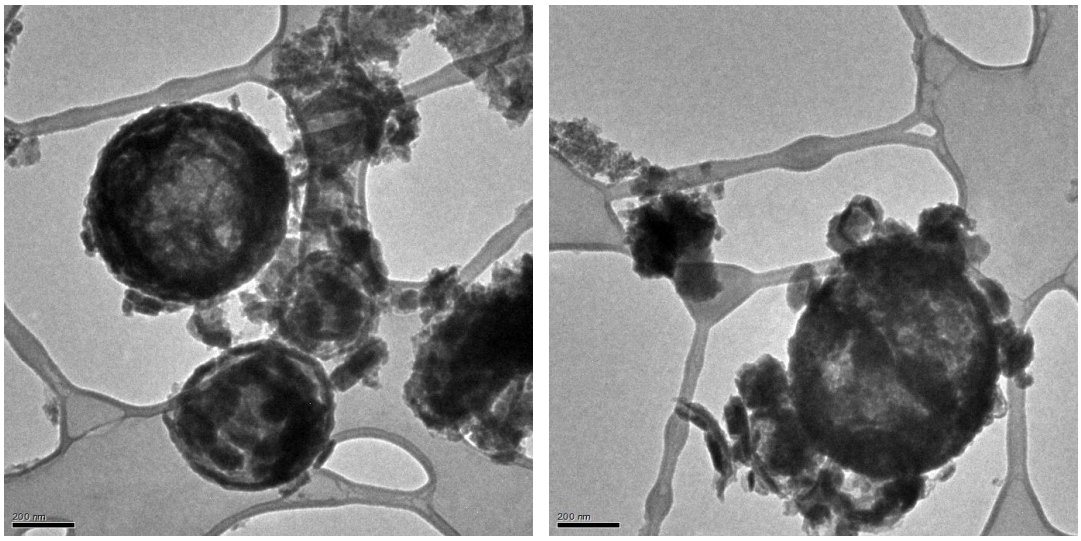

Figure 36. TEM images of samples after etching.

Here I tried to reduce the NaOH concentration and increase the etching time. But the result is still not good. The peak of LFP will disappear with the peak of SiO_2. $LiFePO_4$ slightly changes upon aging in water[34]. So I tried to dissolve the NaOH pellets in ethyl alcohol. 10 g NaOH and 500 mL ethyl alcohol are mixed then try to etch the samples. Figure 37 (a) and (b) are two contrastive XRD patterns. The result of Figure 37 (b) shows the peaks of lithium iron phosphate was saved. But the peaks of SiO_2 was saved. Figure 37 (c) is the TEM image of the NaOH/ethyl alcohol etching samples. The results show there is space in the center of the sphere. And the

crystal structure is found on the edge of the sphere. But the number of hollow spheres is less. Most of the sphere particles are still like Figure 35 which display solid spheres.

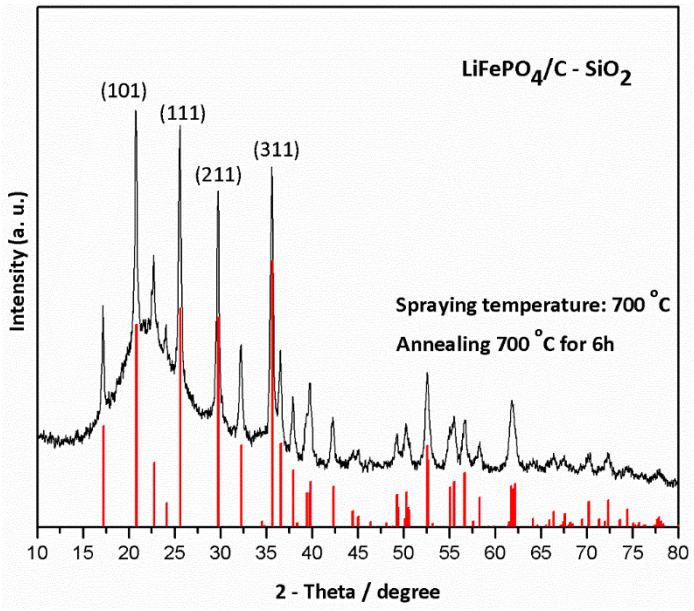

Figure 37 (a). XRD pattern of LFP/C-SiO_2 before etching.

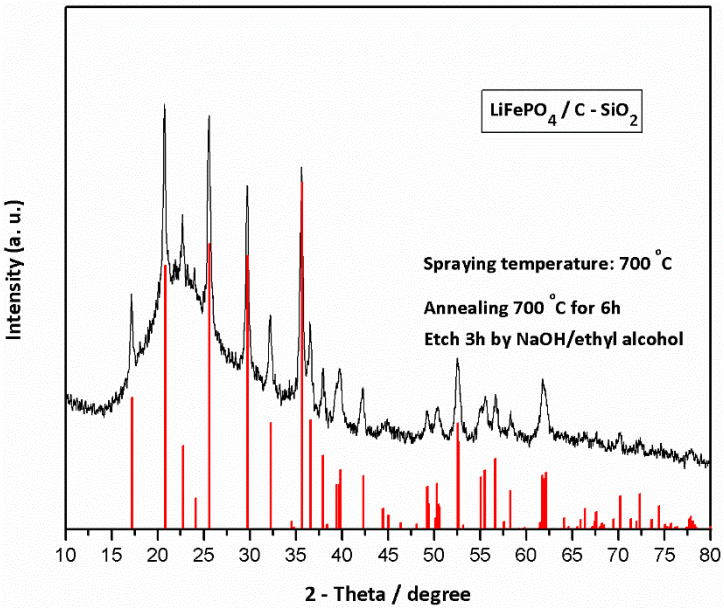

Figure 37 (b). XRD pattern of LFP/C-SiO_2 after etching using NaOH in ethyl alcohol.

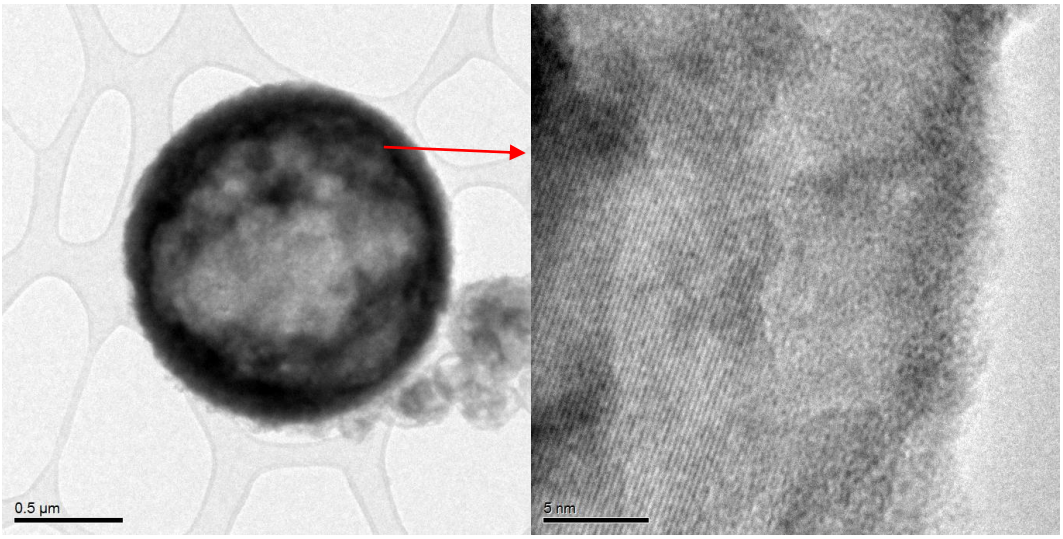

Figure 37 (c). TEM images of LFP/C-SiO_2 after etching using NaOH in ethyl alcohol.

3.6 Morphology of $LiFePO_4$

3.6.1 Scanning electron microscope and EDS mapping

Scanning electron microscope (SEM) is a type of electron microscope. A focused beam of electrons scan the samples then produce images. To prepare the SEM samples, there are two substrates can be chosen. One is carbon film, another is silicon wafer. The silicon wafer is better to observe the morphology. Figure 38 is the SEM image which is used silicon wafer as the substrate. The background is smooth enough to observe the morphology. Figure 39 is the SEM which carbon film was used as the support.

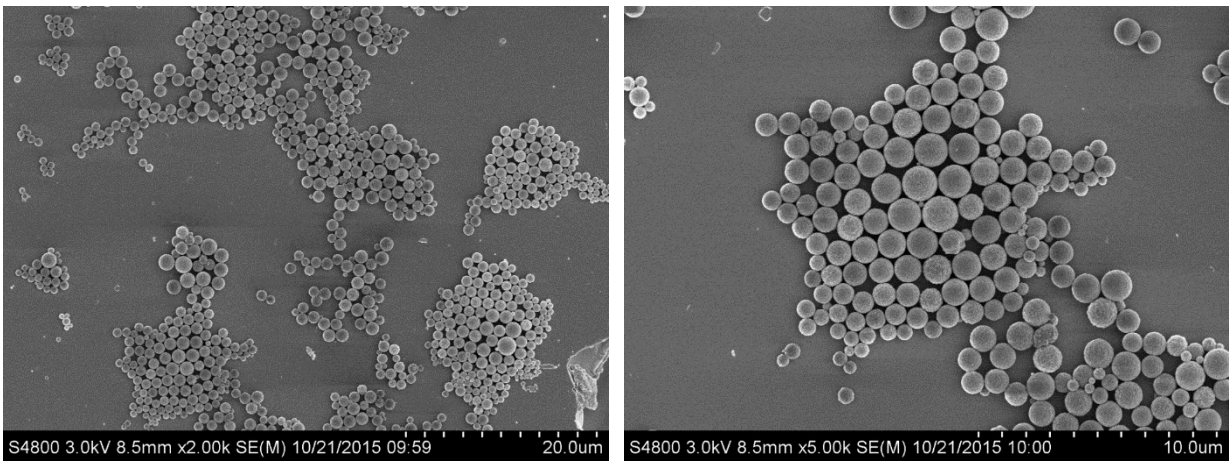

Figure 38. Low-magnification images of the LFP/C-SiO_2 based on silicon wafer.

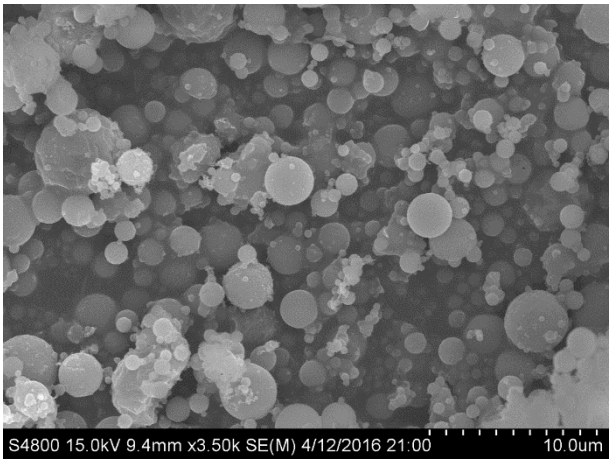

Figure 39. Low-magnification image of the LFP/C-SiO_2 based on carbon film.

From the SEM result, the big size can arrive to 5 micrometer and the small size particles is less than 1 micrometer. The accurate particle size will be detected by transmission electron microscopy later.

EDS mapping of the SEM can detect the element distribution. Figure 40 is the SEM-EDS mapping of one single particle which substrate is carbon film. Figure 41 is the SEM-EDS mapping of the samples based on the silicon film. The element scanned are oxide, iron, phosphorus, and

silicon because these element compose $LiFePO_4$/C-SiO_2. Lithium is too weak to be scanned by SEM. The result shows all elements form a sphere shape. These SEM images result can prove that the LFP/C-SiO_2 has been synthesized as a spherical shape.

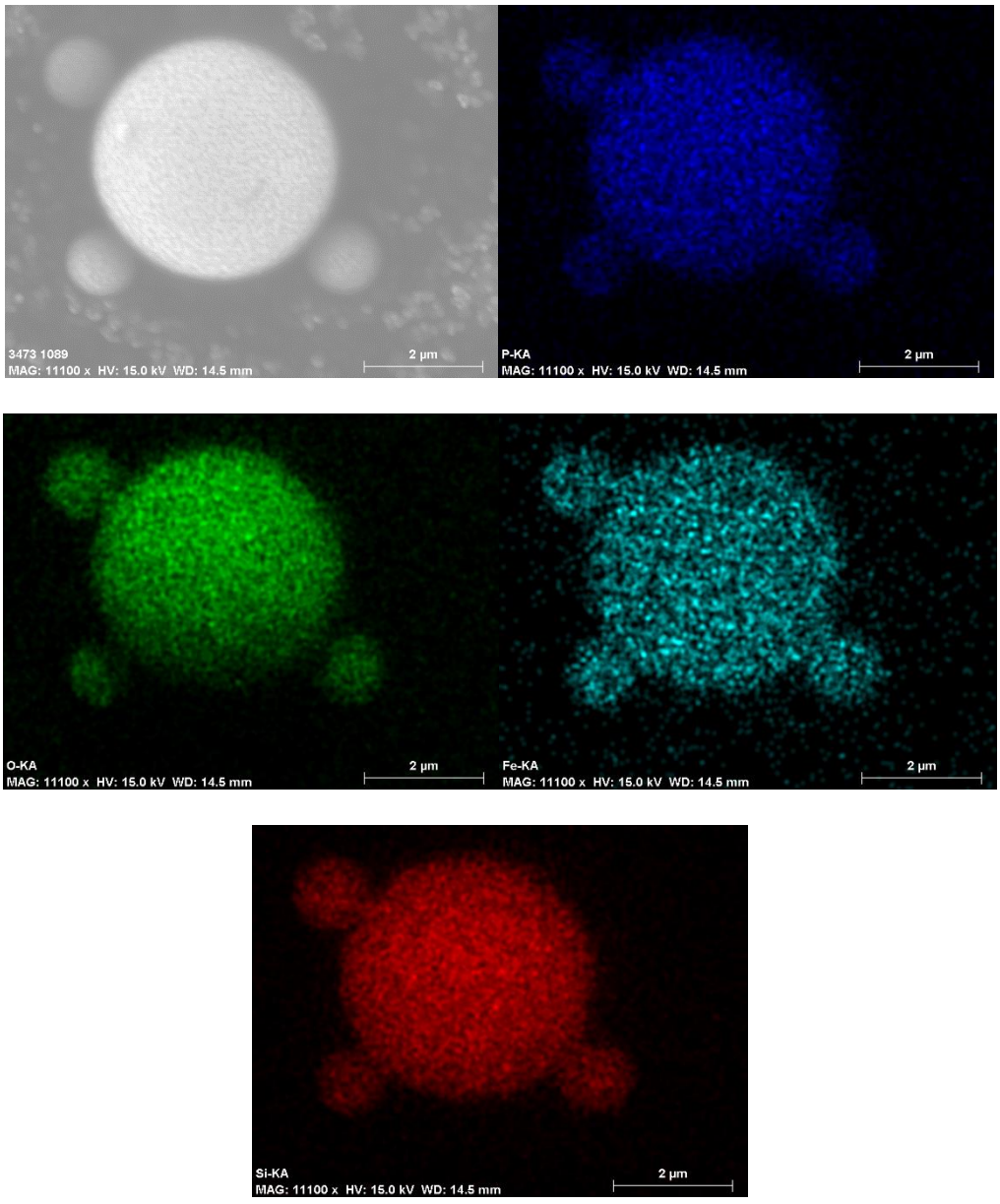

Figure 40. SEM-EDS mapping of the sample based on carbon film.

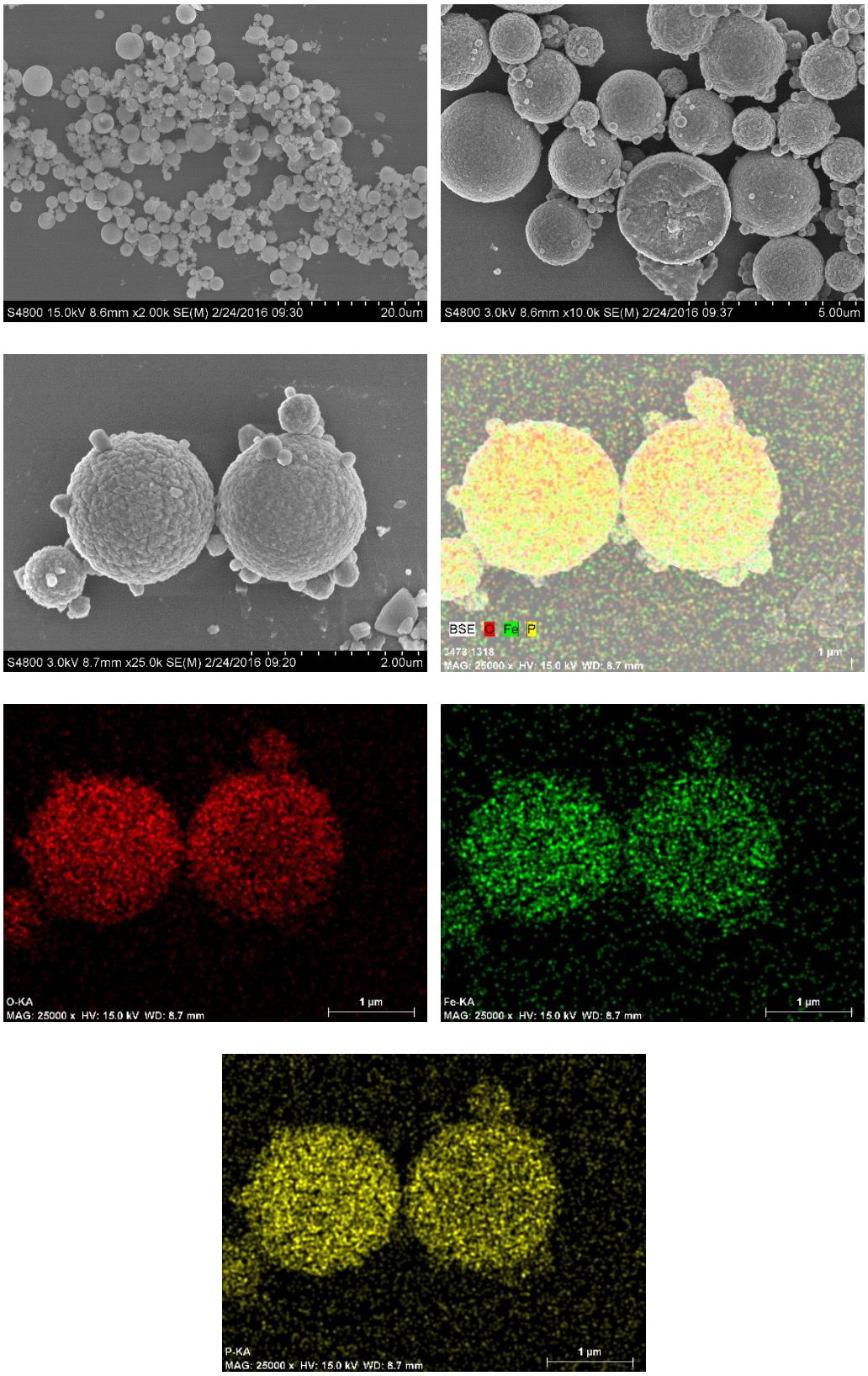

Figure 41. SEM-EDS mapping of the sample based on silicon wafer.

3.6.2 Transmission electron microscopy

The high-resolution transmission electron microscopy uses both the transmitted and the scattered beams to create an interference image[35]. Figure 42 (b) is a HRTEM image. The scale bar is 2 nm. The lattice fringe of LFP can be observed.

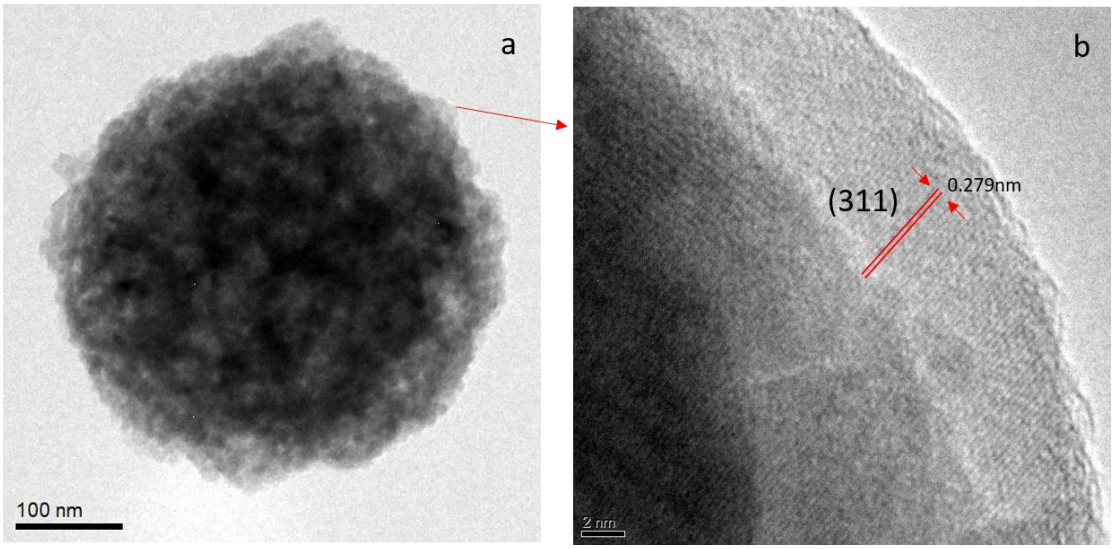

Figure 42. TEM and HRTEM images.

3.7 Electrochemical performance

LFP cathode materials should have 3.4 V flat potential and 170 $mAhg^{-1}$ theoretical capacity during charge/discharge process. From Figure 43 (a) the coin-cell test data, the voltage platform is around 3.4 V. This character shows the cathode material is LFP. The real capacity does not reach to the theoretical capacity. It is around 90 $mAhg^{-1}$ capacity. The capacity of one coin-cell battery is depended on the reactive materials in it. Here, the reactive materials is LFP. But the cathode materials is consist of LFP/C and SiO_2. The SiO_2 templates are still in it and its weight is higher than

LFP/C. So that is the possible reason to explain why the capacity is such low. The Figure 43 (b) display the curve about the cycle number and capacity. It displays the life of coin-cell has more than 200 cycles and it is still working.

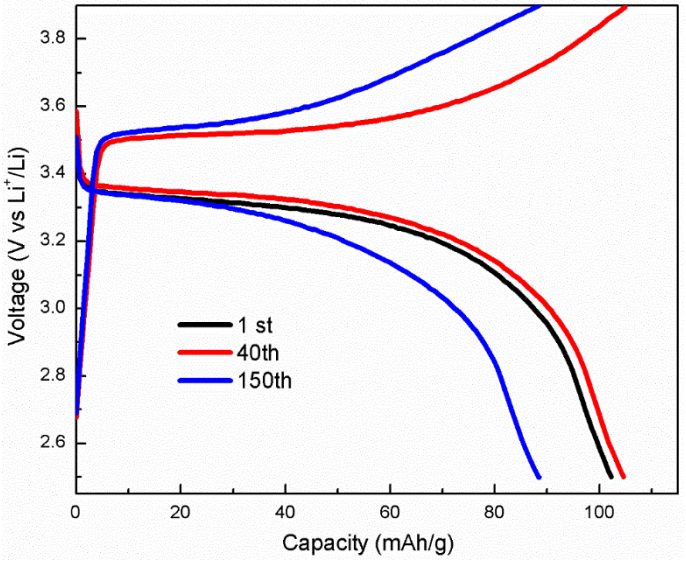

Figure 43 (a). Charge/discharge profile of the coin-cell performance.

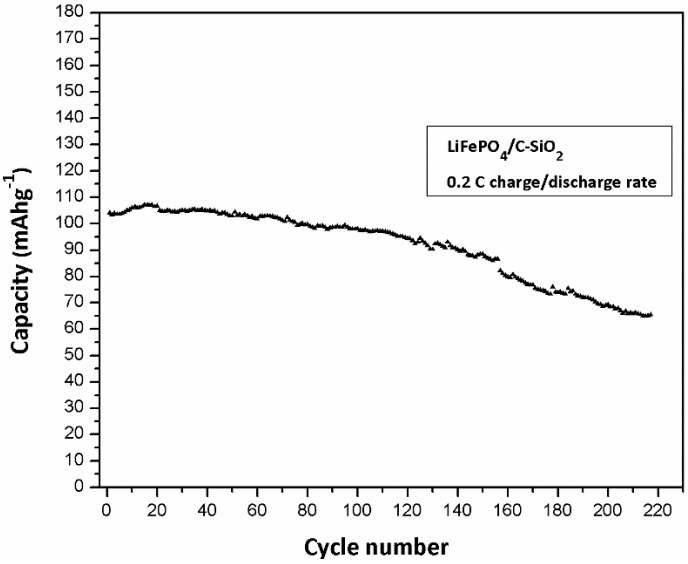

Figure 43 (b). Cycling performance.

Figure 44 shows the initial cyclic voltammetry (CV) performance of the LFP/C-SiO_2. The synthesized conditions are 5 mL SiO_2 templates, 700 °C spraying temperature, and 700 °C annealing temperature. Cyclic voltammetry (CV) is a common technique to study the properties of an electrochemical system that a cyclic linear potential sweep is imposed onto the electrode and the resulting current is recorded[4]. It is often used to study the lithium battery system. The normalized CV profiles do the comparison between the active mass of each electrode with different thicknesses and loadings. From Figure 44, the midpoint of the anodic and cathodic peaks is 3.4 V, which corresponds to the voltage of LFP.

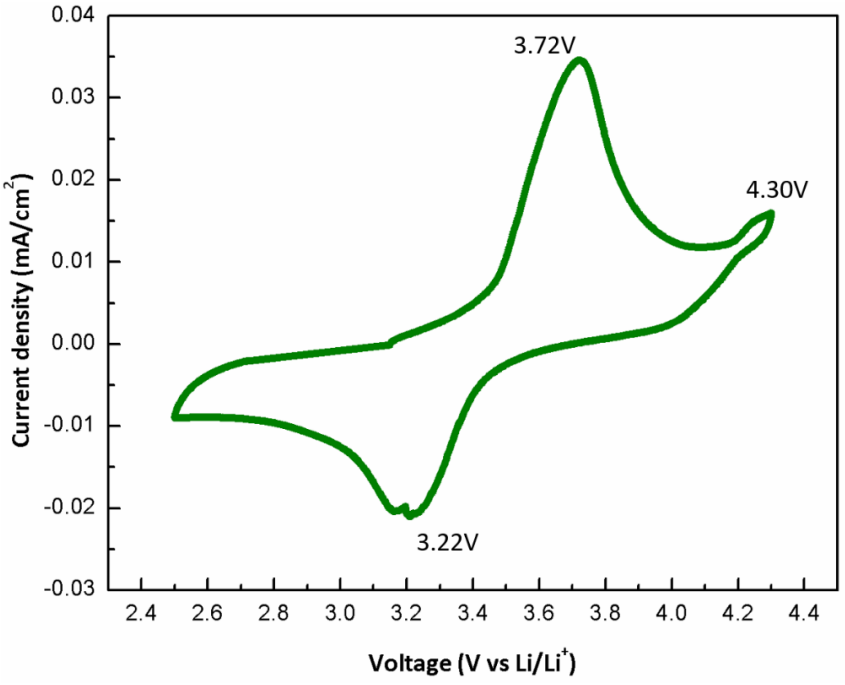

Figure 44. Cyclic voltammetry performance of the LFP/C-SiO_2.

3.8 Transmission X-ray microscopy

The delithiation reaction in lithium ion batteries is often accompanied by an electrochemically driven phase transformation process[36]. Here, the in-situ phase transformation of LFP in a nano-battery was investigated via transmission X-ray microscopy (TXM). This hard X-ray microscopy can offer nanoscale resolution, deep penetration, taking advantage of elemental, and chemical sensitivity[36]. The TXM spectroscopy and nano-tomography with hard X-ray are conducted at beamline 8 BMB, Argonne National Laboratory. Here special thanks for Dr. Junjie Niu, Dr. Jiajun Wang and Yan Zhang to help me to have this chance to use the beamline to detect my samples. Figure 45 and Figure 46 are the TXM sketch.

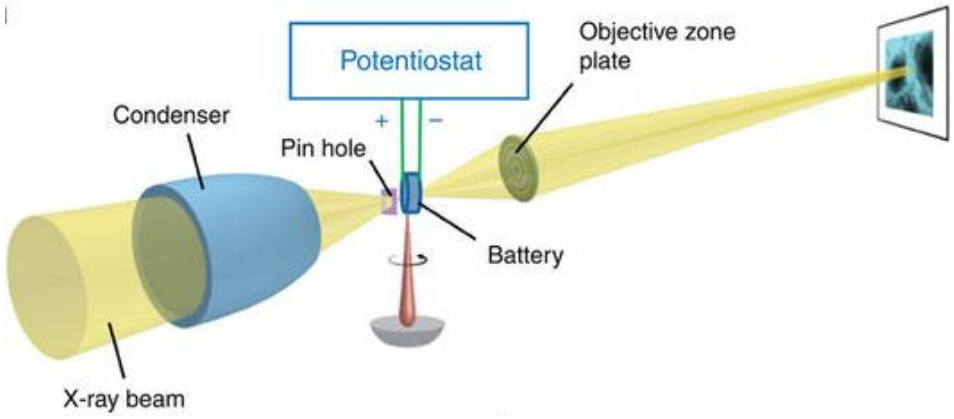

Figure 45. Transmission X-ray microscopy.[36]

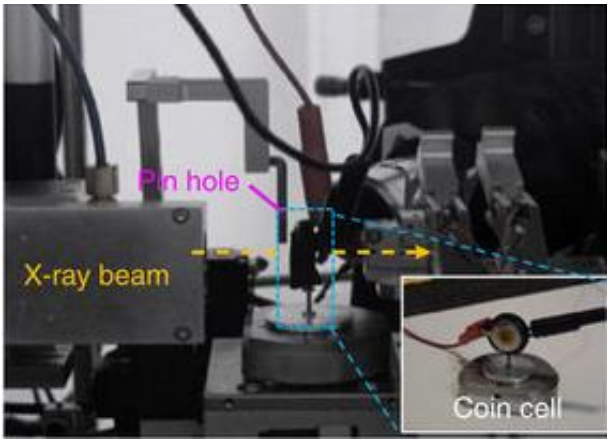

Figure 46. The image of the TXM set-up.[36]

TXM spectroscopy can track the phase transformation in-situ during charge/discharge. A perforated coin cell used for the operando study like Figure 47. The difference between the perforated coin cell and common coin cell is the case of the cell. For the TXM perforated coin cell, the case has a Kapton window on it. That helps the beam line can go through the center of the battery that can help us to detect the transformation during charge/discharge process. The operando cell containing the LFP as cathode electrode. It can also scan the powder samples and produce the 3D image and video.

Figure 47. Nano-battery for the TXM test.

Figure 48 is the needle tip where the LFP/C-SiO_2 powder samples is attached on it. The beam will scan the powders with the tip rotating. The 3D images will be produced on the computer screen. Figure 49 is the 3D images of LFP/C-SiO_2.

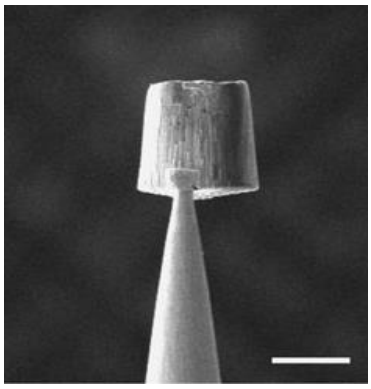

Figure 48. Needle tip where powder sample is attached on.

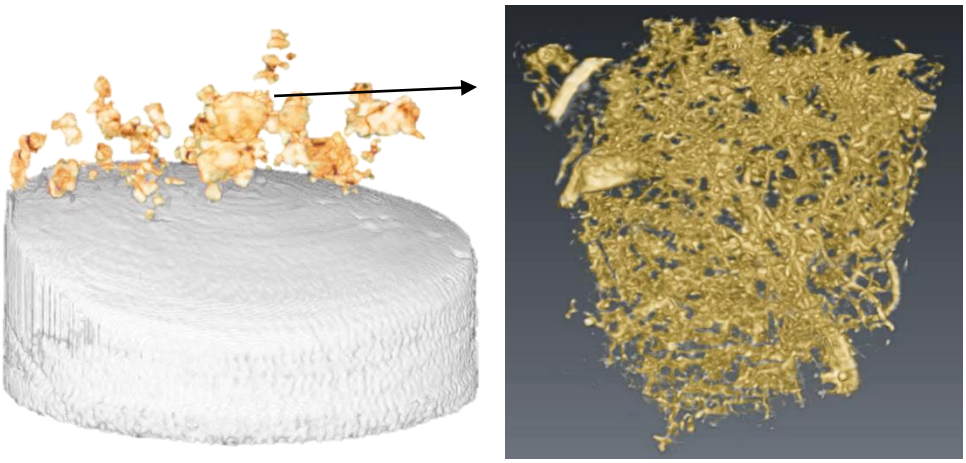

Figure 49. 3D images of LFP/C-SiO_2 from TXM.

Figure 50 shows the composition and 2-dimensional chemical mapping at the phase transformation process during dilithiation/lithiation process. It provides the distribution

information of the area particles during the charge process. Red zone is $LiFePO_4$. Green zone is $FePO_4$.

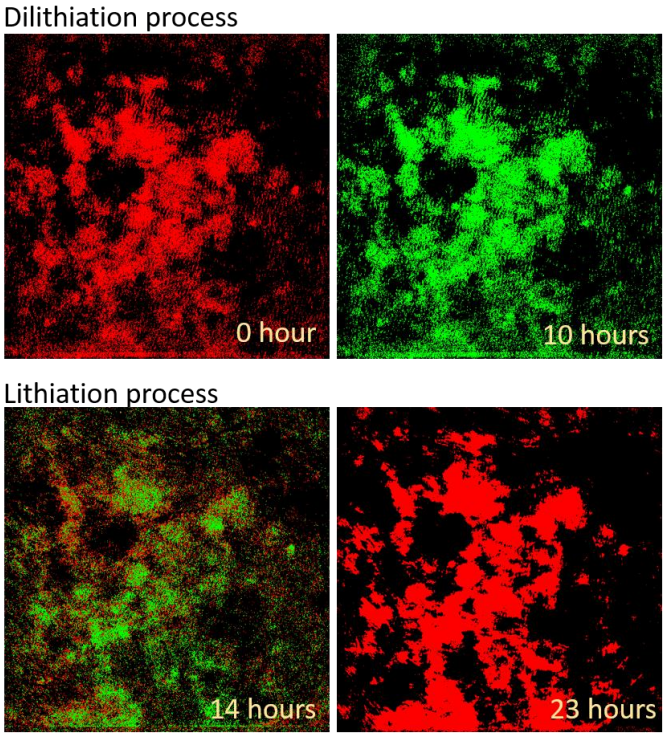

Figure 50. The phase transformation and 2-dimensional chemical mapping of the LFP/FP.

The 2D chemical phase maps show a continued phase transformation from red zone to green zone then transfer back from green to red at the end of the process. From the mapping, the phase transformation is not homogeneous. Two phases that $LiFePO_4$ (red) and $FePO_4$ (green) were found at the same time. At 0 hours, all phase in the area is $LiFePO_4$. During the charge process, $FePO_4$ phase becomes more and more but $LiFePO_4$ can still be observed. Some particles has changed to $FePO_4$ completely and coexist with $LiFePO_4$ particles. At 10 hours, all particles were completely

changed to $FePO_4$ phases. At 14 hours, this concomitant phenomenon is much more obvious. And the phase transformation begin to overturn from $FePO_4$ (greed zone) to $LiFePO_4$ (red zone). Between the $LiFePO_4$ and $FePO_4$ phases during the process, there should be a mixed phase zones which is either fully $LiFePO_4$ or fully $FePO_4$ which proposed by Jiajun Wang's research[36]. Here the yellow zone didn't be observed and the reasonable explanation is that the time interval to produce each mapping it too long. For the future experiment, produce chemical mapping every 10minutes even seconds will get more useful information.

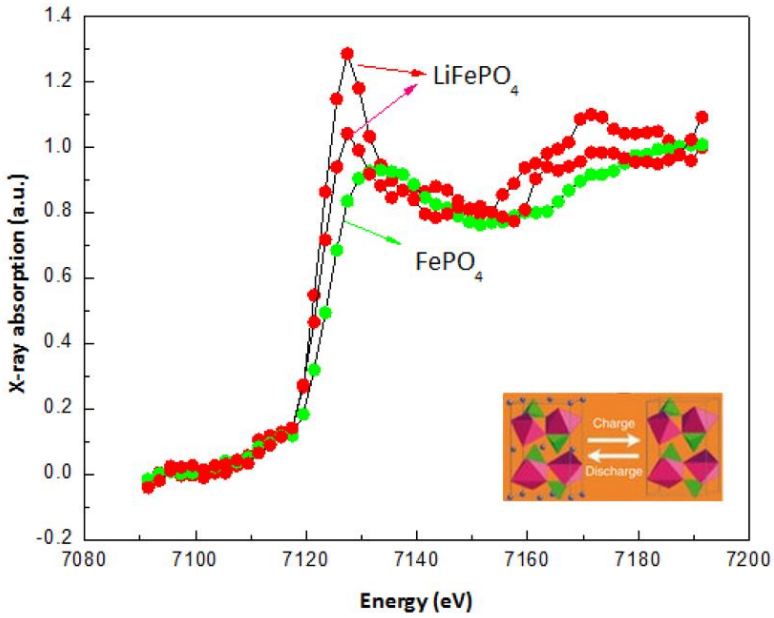

Figure 51. X-ray absorption near edge structure (XANES).

Here is the charge state diagram of one region which is Figure 51. From this diagram, the sharpest peak is the origin $LiFePO_4$ before dilithiation process. With the phases changing from $LiFePO_4$ to $FePO_4$, the chemical sensitive for the X-ray absorption will change too. So when the

phases transfer to $FePO_4$, the X-ray absorption diagram show like the green line. When the phases transfer back to $LiFePO_4$, the Y-axis of the curve should also be back to the same level just like the first sharpest curve.

The conclusion of the TXM study can be summarized as three points. 1. Visualization of surface phase changes occurring at the interface: $LiFePO_4$ and $FePO_4$ phases in a same region. 2. The two phases of $LiFePO_4$ to $FePO_4$ are marked with two different colors. 3. Series of XANES spectra show energy changes of two phases during lithiation/delithiation.

Chapter 4 – Conclusions

In this study, we used a simple method to synthesize sphere $LiFePO_4$/C-SiO_2 nano materials. The spraying method using nebulizer and CVD furnace is much simpler. The conditions we found:

1. The sucrose is necessary because not only it is the source of the carbon, but also it will support the annealing process to synthesize LFP.
2. In this method, the content of silicon dioxide determines the size of the particles.
3. The sample received the better crystalize structure under the 700 °C spraying temperature and 700 °C annealing temperature with 6 hours annealing time.

The crystal lattice and sphere structure were confirmed by XRD, SEM, and TEM, respectively. The size of the sphere is from 300 nm to 3 μm. This size is not uniform because the SiO_2 template will agglomerate. From the XRD patterns, the LFP's peaks can be observed clearly. SEM and TEM show the sphere form and lattice fringe clearly. All of these characteristics help us to confirm the synthesis of LFP is successful.

The LFP/C-SiO_2 exhibits the unique performance of LFP batteries such as the 3.4 voltage charge/discharge platform. The cycle life is over 200 cycles. The capacity can reach around 60-100 $mAhg^{-1}$. This is because the silicon dioxide in the cathode materials was not completely removed. In cathode materials, the silicon dioxide is not conductive. This will affect the performance of the battery.

From the transmission X-ray microscopy results, the phase transformation mechanism of $LiFePO_4$/C-SiO_2 was investigated. During the charge/discharge, we found two phases of

$LiFePO_4/FePO_4$ and a metastable phase exit spontaneously which may depend on the crystallographic orientations. This TXM study can support us to study the mechanism of the LFP charge/discharge process.

Chapter 5 – References

[1] S. Ramdon, B. Bhushan, and S. C. Nagpure, In situ electrochemical studies of lithium-ion battery cathodes using atomic force microscopy, Journal of power sources, 2014, 249, 373.

[2] S. C. Nagpure, and B. Bhushan, In applied scanning probe methods XIII, Springer, 2009, 203.

[3] B. Wu, N. Li, and Y. Ren, $LiFePO_4$ cathode material, INTECH open access publisher, 2011.

[4] D. Y. W. Yu, C. Fietzek, W. Weydanz, K. Donoue, T. Inoue, H. Kurokawa, and S. Fujitani, Study of $LiFePO_4$ by cyclic voltammetry, Journal of the electrochemical society, 2007, 154, A253.

[5] N. Nitta, and G. Yushin, High-capacity anode materials for lithium-ion batteries: choice of elements and structures for active particles, Particle & particle systems characterization, 2014, 31, 317.

[6] N. Nitta, F. Wu, J. T. Lee, and G. Yushin, Li-ion battery materials: present and future, Materials today, 2015, 18, 252.

[7] M. C. Julien, A. Mauger, K. Zaghib, and H. Groult, Comparative issues of cathode materials for Li-ion batteries, Inorganics, 2014, 2.

[8] A. Du Pasquier, I. Plitz, S. Menocal, and G. Amatucci, A comparative study of Li-ion battery, supercapacitor and nonaqueous asymmetric hybrid devices for automotive applications, Journal of power sources, 2003, 115, 171.

[9] K. S. Nanjundaswamy, A. K. Padhi, J. B. Goodenough, S. Okada, H. Ohtsuka, H. Arai, and J. Yamaki, Synthesis, redox potential evaluation and electrochemical characteristics of NASICON-related-3D framework compounds, Solid state ionics, 1996, 92, 1.

[10] A. K. Padhi, K. S. Nanjundaswamy, and J. B. D. Goodenough, Phospho-olivines as positive-electrode materials for rechargeable lithium batteries, Journal of the electrochemical society, 1997, 144, 1188.

[11] Y. Huang, H. Liu, Y.-C. Lu, Y. Hou, and Q. Li, Electrophoretic lithium iron phosphate/reduced graphene oxide composite for lithium ion battery cathode application, Journal of power sources, 2015, 284, 236.

[12] S.-Y. Chung, J. T. Bloking, and Y.-M. Chiang, Electronically conductive phospho-olivines as lithium storage electrodes, Nature materials, 2002, 1, 123.

[13] N. Meethong, H.-Y. S. Huang, W. C. Carter, and Y.-M. Chiang, Size-dependent lithium miscibility gap in nanoscale $Li_{1-x}FePO_4$, Electrochemical and solid-state letters, 2007, 10, A134.

[14] T. F. Yi, X. Y. Li, H. Liu, J. Shu, Y. R. Zhu, and R. S. Zhu, Recent developments in the doping and surface modification of $LiFePO_4$ as cathode material for power lithium ion battery, Ionics, 2012, 18, 529.

[15] J. J. Niu, A. Kushima, X. Qian, L. Qi, K. Xiang, and Y. M. Chiang, J. Li, In situ observation of random solid solution zone in $LiFePO_4$ electrode, Nano letters, 2014, 14, 4005.

[16] S. Yang, M. Hu, L. Xi, R. Ma, Y. Dong, and C. Y. Chung, Solvothermal synthesis of monodisperse $LiFePO_4$ micro hollow spheres as high performance cathode material for lithium ion batteries, ACS applied materials & interfaces, 2013, 5, 8961.

[17] J. Wang, and X. Sun, Understanding and recent development of carbon coating on $LiFePO_4$ cathode materials for lithium-ion batteries, Energy & environmental science, 2012, 5, 5163.
[18] J. H. Shin, W. A. Henderson, S. Scaccia, P. P. Prosini, and S. Passerini, Solid-state Li/$LiFePO_4$ polymer electrolyte batteries incorporating an ionic liquid cycled at 40°C, Journal of power sources, 2006, 156, 560.
[19] L. X. Yuan, Z. H. Wang, W. X. Zhang, X. L. Hu, J. T. Chen, Y. H. Huang, and J. B. Goodenough, Development and challenges of $LiFePO_4$ cathode material for lithium-ion batteries, Energy environ. Sci. 2011, 4, 269.
[20] L. Laffont, C. Delacourt, P. Gibot, M. Y. Wu, P. Kooyman, C. Masquelier, and J. M. Tarascon, Study of the $LiFePO_4/FePO_4$ two-phase system by high-resolution electron energy loss spectroscopy, Chemistry of materials, 2006, 18, 5520.
[21] C. Delmas, M. Maccario, L. Croguennec, F. Le Cras, and F. Weill, Lithium deintercalation in $LiFePO_4$ nanoparticles via a domino-cascade model, Nature materials, 2008, 7, 665.
[22] J. Liu, T. E. Conry, X. Song, M. M. Doeff, and T. J. Richardson, Nanoporous spherical $LiFePO_4$ for high performance cathodes, Energy environ. Sci. 2011, 4, 885.
[23] L. Yu, D. Cai, H. Wang, and M. M. Titirici, Synthesis of microspherical $LiFePO_4$-carbon composites for lithium-ion batteries, Nanomaterials, 2013, 3, 443.
[24] Z. D. Huang, S. W. Oh, Y. B. He, B. Zhang, Y. Yang, Y. W. Mai, and J. K. Kim, Porous C-$LiFePO_4$-C composite microspheres with a hierarchical conductive architecture as a high performance cathode for lithium ion batteries, Journal of materials chemistry, 2012, 22, 19643.
[25] B. Ellis, W. H. Kan, W. R. M. Makahnouk, and L. F. Nazar, Synthesis of nanocrystals and morphology control of hydrothermally prepared $LiFePO_4$, Journal of materials chemistry 2007, 17, 3248.
[26] M. Sanchez, G. Brito, M. Fantini, G. Goya, and J. Matos, Synthesis and characterization of $LiFePO_4$ prepared by sol-gel technique, Solid state ionics, 2006, 177, 497.
[27] B. Jin, and Q. Jiang, $LiFePO_4$ Cathode materials for lithium-ion batteries, ChemInform, 2011, 42.
[28] C. Zhao, L. Liu, H. Zhao, A. Krall, Z. Wen, J. Chen, P. Hurley, J. Jiang, and Y. Li, Sulfur-infiltrated porous carbon microspheres with controllable multi-modal pore size distribution for high energy lithium-sulfur batteries, Nanoscale, 2014, 6, 882.
[29] K. Wang, R. Cai, T. Yuan, X. Yu, R. Ran, and Z. Shao, Process investigation, electrochemical characterization and optimization of $LiFePO_4$/C composite from mechanical activation using sucrose as carbon source, Electrochimica Acta, 2009, 54, 2861.
[30] Y. Liu, W. Zhang, J. Jiang, D. Ma, and H. Wang, Structure and electrochemical characteristics of $LiFePO_4$ synthesized by hydrothermal method with different carbon resources, Journal of materials science and engineering, 2012, B2(4), 255.
[31] J. Yang, J. Wang, D. Wang, X. Li, D. Geng, G. Liang, M. Gauthier, R. Li, and X. Sun, 3D porous $LiFePO_4$/graphene hybrid cathodes with enhanced performance for Li-ion batteries, Journal of power sources, 2012, 208, 340.

[32] C. M. Doherty, R. A. Caruso, B. M. Smarsly, P. Adelhelm, and C. J. Drummond, Hierarchically porous monolithic $LiFePO_4$/carbon composite electrode materials for high power lithium ion batteries, Chemistry of materials, 2009, 21, 5300.
[33] S. Lim, C. S. Yoon, and J. Cho, Synthesis of nanowire and hollow $LiFePO_4$ cathodes for high-performance lithium batteries, Chemistry of materials, 2008, 20, 4560.
[34] W. Porcher, P. Moreau, B. Lestriez, S. Jouanneau, F. Le Cras, and D. Guyomard, Stability of $LiFePO_4$ in water and consequence on the Li battery behaviour, Ionics, 2008, 14, 583.
[35] F. L. Deepak, A. Mayoral, and R. Arenal, Advanced transmission electron microscopy, Springer international publishing switzerland, 2015.
[36] J. J. Wang, Y-C. K. C-Wiegart, and J. Wang, In operando tracking phase transformation evolution of lithium iron phosphate with hard X-ray microscopy, Nature communications, 2014, 5, 4570.